

Received: 18 February 2012 – Accepted: 17 May 2012 – Published: 30 May 2012

Correspondence to: M. Kajino (kajino@mri-jma.go.jp)

Published by Copernicus Publications on behalf of the European Geosciences Union.

ACPD

12, 13405–13456, 2012

**Development of
RAQM2 and Asian
aerosol mixing type
simulation**

M. Kajino et al.

Title Page

Abstract

Introduction

Conclusions

References

Tables

Figures



Back

Close

Full Screen / Esc

Printer-friendly Version

Interactive Discussion



Abstract

A new aerosol chemical transport model, Regional Air Quality Model 2 (RAQM2), was developed to simulate Asian air quality. We implemented a simple version of a modal-moment aerosol dynamics model (MADMS) and achieved a completely dynamic (non-equilibrium) solution of a gas-to-particle mass transfer over a wide range of aerosol diameters from 1 nm to super μm . To consider a variety of atmospheric aerosol properties, a category approach was utilized, in which the aerosols were distributed into 4 categories: Aitken mode (ATK), soot-free accumulation mode (ACM), soot aggregates (AGR), and coarse mode (COR). Condensation, evaporation, and Brownian coagulations for each category were solved dynamically. A regional-scale simulation ($\Delta x = 60\text{ km}$) was performed for the entire year of 2006 covering the North-east Asian region. Statistical analyses showed that the model reproduced the regional-scale transport and transformation of the major inorganic anthropogenic and natural air constituents within factors of 2 to 5. The modeled PM_{10} /bulk ratios of the chemical components were consistent with the observations, indicating that the simulations of aerosol mixing types were successful. Non-sea salt SO_4^{2-} mixed with ATK + ACM was the largest at Hedo in summer, whereas it mixed with AGR was substantial in cold seasons. Ninety-eight percent of the modeled NO_3^- was mixed with sea salt at Hedo, whereas 53.7% of the NO_3^- was mixed with sea salt at Gosan, located upwind toward the Asian continent. The condensation of HNO_3 onto sea salt particles during transport over the ocean makes the difference in the NO_3^- mixing type at the two sites. Because the aerosol mixing type alters optical properties and cloud condensation nuclei activity, its accurate prediction and evaluation are indispensable for aerosol-cloud-radiation interaction studies.

Development of RAQM2 and Asian aerosol mixing type simulation

M. Kajino et al.

Title Page

Abstract

Introduction

Conclusions

References

Tables

Figures

⏪

⏩

◀

▶

Back

Close

Full Screen / Esc

Printer-friendly Version

Interactive Discussion



1 Introduction

Atmospheric trace gases and aerosols have various detrimental effects on ecosystems and human health. Because their emission, secondary formation, transport and deposition mechanisms are highly complex and still unknown, a great number of studies on the development and application of air quality modeling are ongoing. Recently, Jacobson and Ginnebaugh (2010) developed a global-through-urban nested three-dimensional air pollution model that implements a large explicit photochemical mechanism with 4675 gases and 13 626 tropospheric and stratospheric chemical reactions. The mechanism also includes one internally mixed aerosol and three hydrometeor categories that are size and chemistry resolved (17 components \times 14 size bins for aerosols, 18 components \times 30 size bins for cloud/precipitation liquid, cloud/precipitation ice, cloud/precipitation graupel). On the other hand, there is still a high demand for computationally efficient models for the purpose of long-term integration with higher grid resolutions. For example, the Community Multiscale Air Quality (CMAQ) model (Byun and Schere, 2006) was extensively used worldwide and was continually updated for more than 10 yr to the current version 4.7 (Foley et al., 2010).

Asian air quality is highly complex because it covers the tropics to the polar zones with huge amounts of anthropogenic air pollutants and natural Asian dust particles together with other natural species. The Regional Air Quality Model (RAQM) was developed at the Acid Deposition and Oxidant Research Center (currently changed to the Asia Center for Air Pollution Research), which focuses on such Asian air quality problems (An et al., 2002; Han, 2007). The model has been used for various air pollution studies in Asia, such as studies on high oxidant, massive dust transport, and volcanic sulfur episodes, and substantial modifications have been made based on comparison and evaluation with extensive and long-term monitoring data (An et al., 2002, 2003; Han, 2007; Han et al., 2004, 2005, 2006; Kajino et al., 2004, 2005) and with other models (Carmichael et al., 2008 and references therein). However, an aerosol dynamics module was not implemented in RAQM, and thermodynamic equilibrium was assumed

ACPD

12, 13405–13456, 2012

Development of RAQM2 and Asian aerosol mixing type simulation

M. Kajino et al.

Title Page

Abstract

Introduction

Conclusions

References

Tables

Figures

⏪

⏩

◀

▶

Back

Close

Full Screen / Esc

Printer-friendly Version

Interactive Discussion

for the gas-aerosol partitioning of semi-volatile inorganic components such as sulfate, nitrate and ammonium.

To simulate the evolutionary processes of aerosol microscale properties such as chemical compositions, size distribution and mixing state, we implemented a simple version of a new modal-moment aerosol dynamics model (Kajino, 2011; Kajino and Kondo, 2011) that enables the non-equilibrium calculation of gas-to-particle mass transfer over a wide range of aerosol diameters from 1 nm to super-micrometer particles. We also implemented six important parameterizations relating to aerosol dynamics: (1) new particle formation, (2) cloud condensation nuclei (CCN) activation, (3) ice nuclei (IN) activation, (4) an explicit grid-scale cloud microphysical module, (5) dry deposition, and (6) sub-grid-scale convection and scavenging.

The new model is referred to as RAQM2. In Sect. 2, a unique aerosol dynamics module is described in detail together with the above parameterizations. The model results are evaluated in Sect. 3 using the Acid Deposition Monitoring Network in East Asia (EANET) and the Cape Hedo Atmosphere and Aerosol Monitoring Station (CHAAMS). The major findings are summarized in Sect. 4.

2 Model description

2.1 General description of the WRF/RAQM2 framework and parameterizations used in the models

In this section, a general description of an offline-coupled meteorology – chemical transport framework (WRFV3/RAQM2) is presented; however, because the aerosol dynamics model of RAQM2 is unique, it is described in detail in Sect. 2.2. Table 1 summarizes the list of data and schemes used in the WRF and RAQM2 models.

Figure 1 illustrates the model domain of WRF and RAQM2, and the locations of the observation sites of the Acid Deposition Monitoring Network in East Asia (EANET) and the Cape Hedo Atmosphere and Aerosol Monitoring Station (CHAAMS). There are

Development of RAQM2 and Asian aerosol mixing type simulation

M. Kajino et al.

Title Page

Abstract

Introduction

Conclusions

References

Tables

Figures

⏪

⏩

◀

▶

Back

Close

Full Screen / Esc

Printer-friendly Version

Interactive Discussion



**Development of
RAQM2 and Asian
aerosol mixing type
simulation**M. Kajino et al.

[Title Page](#)[Abstract](#)[Introduction](#)[Conclusions](#)[References](#)[Tables](#)[Figures](#)[⏪](#)[⏩](#)[◀](#)[▶](#)[Back](#)[Close](#)[Full Screen / Esc](#)[Printer-friendly Version](#)[Interactive Discussion](#)

horizontally 90×60 grids with 60 km grid resolution on a Lambert conformal map projection. There are vertically 28 layers from the ground to 100 hPa for WRF and 13 layers to 10 km for RAQM2 with terrain-following coordinates. The horizontal grid points are common to both WRF and RAQM2, whereas the vertical grid points are different. After the spline vertical interpolation of wind velocity and air density to the RAQM2 levels, the mass balance is not maintained. Thus, the mass continuity model MSCWM (Ishikawa, 1994) is used to reduce the mass divergence due to the vertical interpolation to about 10^{-5} to 10^{-6} (s^{-1}). The input/output time interval for WRF-RAQM2 was set to 1 h. For the lateral and upper boundary concentrations of the RAQM2 simulation, the climatological simulation results of monthly NO_x , O_x , CO and volatile organic compound (VOC) concentrations were used using a global-scale stratospheric and tropospheric chemistry climate model (MRI-CCM2; Deushi and Shibata, 2011). The entire simulation period was 1 yr, but each simulation was performed separately for each month, with a spin-up period of 2 weeks.

RAQM2 incorporates major processes for atmospheric trace species, such as anthropogenic and natural emissions, advection, turbulent diffusion, photochemistry, new particle formation, condensation, evaporation, Brownian coagulation, dry deposition, grid-scale cloud condensation nuclei (CCN) and ice nuclei (IN) activation and subsequent cloud microphysical processes, grid-scale aqueous chemistry in hydrometeors as well as in aerosol water, subgrid-scale convection and wet scavenging (Table 1).

The emission inventory was obtained from REAS (Ohara et al., 2007), which was extended to the year 2005 (Kurokawa et al., 2009). The emitted species are NO_x , SO_2 , NH_3 , NMVOCs (Non-Methane Volatile Organic Compounds), BC (Black Carbon), and POAs (Primary Organic Aerosols). Because REAS does not provide seasonal variations of the emission flux, we applied the simple monthly variations for Chinese emissions (Table 9 of Zhang et al., 2009). The temporal variations of the anthropogenic emission flux are not considered in the current setting. We used the Global Fire Emissions Database (GFED3; Giglio et al., 2010) for open biomass burning emissions (NO_x , SO_2 , NMVOCs, BC and, POA) and the Model of Emissions of Gases and Aerosols from

Nature (MEGAN2; Guenther et al., 2006) for biogenic emissions (isoprene and terpenes). Clarke et al. (2006) was used for sea salt production and Han et al. (2004) for the dust deflation process. The fractions of crustal elements such as Na^+ , Ca^{2+} , Mg^{2+} , and K^+ in sea salt and Asian dust particles are derived from Song and Carmichael (2001). However, using the above combinations, the PM_{10} and non-sea salt (nss) Ca^{2+} were overestimated during the dust transport season in spring 2006 in Japan. There have been substantial efforts to adjust dust emission flux and transport by developing sophisticated physical deflation models (Kang et al., 2011, and references therein) or by applying state-of-the-art data assimilation techniques (e.g., Yumimoto et al., 2008; Sekiyama et al., 2010). Because deducing the accurate dust emission flux was not a focus of this study, we simply reduced the dust emission to one quarter uniformly in time and in space and the Ca^{2+} contents (6.8 wt%) in the Asian dust to half (3.4 wt%) to roughly adjust to both the observed PM_{10} and the nss- Ca^{2+} concentration at the Japan EANET stations for 2006. The value of 3.4 wt% is smaller than that in previous works, such as Song and Carmichael (2001) and Wang et al. (2002), but the value is still plausible compared with the China-map project data (available at http://www.cgrer.uiowa.edu/EMISSION_DATA/biogeno/Ca-chinamap.gif, last access: 28 May 2012).

The SAPRC99 mechanism (Carter, 2000) was implemented for gas phase photochemistry, together with additional Secondary Organic Aerosol (SOA) formation mechanism (Edney et al., 2007). However, because the contribution of SOA mass produced by the model was found to be less significant to the East Asian regional-scale simulations and because we focused mainly on the behaviors of inorganic components, the process was not included in the current study. The aqueous phase chemistry in grid-scale cloud and rain water droplets as well as aerosol water was considered (Walcek and Taylor, 1986; Carlton et al., 2007). The wet scavenging due to the subgrid-scale convection was considered using the Asymmetrical Convective Model (Pleim and Chang, 1992), whereas aqueous phase chemistry in convective clouds was not considered. Zhang et al. (2003) was used to calculate the dry deposition velocities of

Development of RAQM2 and Asian aerosol mixing type simulation

M. Kajino et al.

Title Page

Abstract

Introduction

Conclusions

References

Tables

Figures

⏪

⏩

◀

▶

Back

Close

Full Screen / Esc

Printer-friendly Version

Interactive Discussion

gaseous species. The monthly composite MODIS/LAI data processed from MOD15A2 (Myneni et al., 2002; Yang et al., 2006) are used to obtain realistic values for the surface resistances of the dry deposition velocity. Aerosol dry deposition is calculated using the method of Zhang et al. (2001) with modifications to improve the prediction accuracy, as described in detail in Sect. 2.2.8.

2.2 Formulations of a fully dynamic aerosol module

The current aerosol module is a three moment bulk dynamics model that conserves number, surface area, and mass concentrations of aerosol populations under the assumption that sizes of aerosols can be represented by uni-modal lognormal size distributions (LNSDs). In this section, an aerosol category approach is introduced that presents dynamical and chemical evolutions in the mass and size distributions of aerosols due to emissions, new particle formation, condensation, Brownian coagulation, dry deposition, CCN activation, IN activation, and cloud microphysical processes using a modal-moment dynamics approach.

2.2.1 Simple version of an aerosol module MADMS

A simple version of an aerosol module called Modal Aerosol Dynamics model for multiple Modes and fractal Shapes (MADMS; Kajino, 2011) was implemented in RAQM2. MADMS can simulate the Brownian coagulation of a couple of modes with very different LNSD parameters and with different mass fractal dimensions (D_f) of aggregates. Simply, in RAQM2, all the particles were assumed to be spherical ($D_f = 3$).

As shown in Table 2, the populations of aerosols were grouped into 4 categories: 1. Aitken mode (ATK); 2. accumulation mode (ACM); 3. soot aggregates (AGR); and 4. coarse mode (COR). The ATK category represents an assemblage of aerosols formed by new particle formation and growing through the coagulation and condensation of trace gases and water vapor. The ACM category includes a part of the ATK aerosols that evolved to be larger than a certain diameter (set as 40 nm in this study) as well

Development of RAQM2 and Asian aerosol mixing type simulation

M. Kajino et al.

Title Page

Abstract

Introduction

Conclusions

References

Tables

Figures

⏪

⏩

◀

▶

Back

Close

Full Screen / Esc

Printer-friendly Version

Interactive Discussion



Development of RAQM2 and Asian aerosol mixing type simulation

M. Kajino et al.

Title Page

Abstract

Introduction

Conclusions

References

Tables

Figures

⏪

⏩

◀

▶

Back

Close

Full Screen / Esc

Printer-friendly Version

Interactive Discussion

as organic compounds and unidentified mass, and it excludes BC particles. The AGR category indicates soot aggregates generated through combustion, and it contains BC particles. Therefore, the ATK and ACM are non-light-absorbing particles, whereas AGR are light-absorbing particles. Without separating the AGR category from the others, the evolution of the mixing state of BC particles cannot be considered, which alters the absorption of solar radiation and the number of CCN particles. The COR category includes mechanically produced natural aerosols such as dust and sea salt particles as well as unidentified components from PM₁₀ emissions.

The aerosol sizes in each category were assumed to be characterized by a unimodal LNSD. Three parameters were used to fix the LNSD: the number concentration N , the geometric mean diameter D_g , and the geometric standard deviation σ_g . In the modal-moment dynamics modeling, the temporal evolutions of the three moments of LNSD due to dynamical and physical processes were solved to fix the LNSD. The k th moment is defined as

$$M_k = \int_{-\infty}^{\infty} D^k n(\ln D) d(\ln D) \quad (1)$$

Applying the Gaussian integral formula to Eq. (1) results in

$$M_k = ND_g^k \exp \left[\frac{k^2}{2} \ln^2 \sigma \right] \quad (2)$$

A list of tracers to fix the LNSD of each category is shown in Table 2. The zeroth and second moments (M_0 , M_2) and the mass concentrations of unidentified components (UIDs), BC, OA (POA plus SOA), dust (DU), sea salt (except chloride) (SS), sulfate, ammonium, nitrate, chloride and water are tracers. By assuming a constant density of each chemical composition, the M_3 of each category was diagnosed. The LNSD of each category was fixed by the three moments, M_0 , M_2 and M_3 . In the only case of the Brownian coagulation process, M_0 , M_3 and M_6 were used to fix the LNSD. More

detailed derivations and descriptions of the modal moment approach are given in previous papers (e.g., Binkowski and Shankar, 1995; Whitby and McMurry, 1997; Kajino, 2011). Only the final forms of the equations, the time derivative terms of the moments, are shown in the current paper.

5 2.2.2 Intra-category Brownian coagulation

The time derivative of moments due to intra-category coagulation in the free-molecular regime can be expressed as

$$\left. \frac{dM_0}{dt} \right|_{\text{fm}} = -bK_{\text{fm}} [M_0M_{0.5} + M_2M_{-1.5} + 2M_1M_{-0.5}] \quad (3a)$$

$$\left. \frac{dM_6}{dt} \right|_{\text{fm}} = 2bK_{\text{fm}} [M_3M_{3.5} + M_5M_{1.5} + 2M_4M_{2.5}] \quad (3b)$$

where $K_{\text{fm}} = \left(\frac{3k_{\text{B}}T}{\rho_p} \right)^{0.5}$, k_{B} is the Boltzmann constant, T is temperature (K), and ρ_p is the particle density. b is an approximation function of σ as

$$b(\sigma) = 1 + 1.2 \exp(-2\sigma) - 0.646 \exp(-0.35\sigma^2) \quad (4)$$

The time derivative terms in the near-continuum regime is

$$\left. \frac{dM_0}{dt} \right|_{\text{nc}} = -K_{\text{nc}} [M_0M_0 + M_1M_{-1} + A\lambda M_0M_{-1} + A\lambda M_1M_{-2}] \quad (5a)$$

$$\left. \frac{dM_6}{dt} \right|_{\text{nc}} = 2K_{\text{nc}} [M_3M_3 + M_4M_2 + A\lambda M_3M_2 + A\lambda M_4M_1] \quad (5b)$$

where $K_{\text{nc}} = \frac{2k_{\text{B}}T}{3\mu}$, $A = 2.492$, μ is the viscosity of air, and λ is the mean free path of air molecules (cm). Finally, the harmonic mean of the time derivative terms in the

free-molecular and near-continuum regimes is applied to cover the full size range of aerosols as

$$\frac{dM_k}{dt} = \frac{dM_k}{dt} \Big|_{\text{fm}} \times \frac{dM_k}{dt} \Big|_{\text{nc}} / \left[\frac{dM_k}{dt} \Big|_{\text{fm}} + \frac{dM_k}{dt} \Big|_{\text{nc}} \right] \quad (6)$$

During the intra-category coagulation, the third moment proportional to the total volume remains unchanged,

$$\frac{dM_3}{dt} = 0 \quad (7)$$

2.2.3 Inter-category Brownian coagulation

Rules for the transfer of the three moments and chemical mass concentrations from one category to another must be predefined for the inter-category coagulation calculations. These rules are listed in Table 3. Basically, the moments and masses are transferred from smaller/simpler categories into larger/multiple-component categories. Assuming that when a particle in category i coagulate with a particle in category j , the merged particle goes into category j (see Table 3), the time derivative terms of the moments in the near-continuum regime can be written as

$$\begin{aligned} \frac{dM_0^i}{dt} \Big|_{\text{nc}} = & -K_{\text{nc}} \left[2M_0^i M_0^j + M_1^i M_{-1}^j + M_{-1}^i M_1^j + A\lambda M_0^i M_{-1}^j + A\lambda M_{-1}^i M_0^j \right. \\ & \left. + A\lambda M_1^i M_{-2}^j + A\lambda M_{-2}^i M_1^j \right] \end{aligned}$$

$$\begin{aligned} \frac{dM_3^i}{dt} \Big|_{\text{nc}} = & -K_{\text{nc}} \left[2M_3^i M_0^j + M_4^i M_{-1}^j + M_2^i M_1^j + A\lambda M_3^i M_{-1}^j + A\lambda M_2^i M_0^j \right. \\ & \left. + A\lambda M_4^i M_{-2}^j + A\lambda M_1^i M_1^j \right] \end{aligned}$$

Development of RAQM2 and Asian aerosol mixing type simulation

M. Kajino et al.

Title Page

Abstract

Introduction

Conclusions

References

Tables

Figures

⏪

⏩

◀

▶

Back

Close

Full Screen / Esc

Printer-friendly Version

Interactive Discussion



$$\left. \frac{dM_6^i}{dt} \right|_{nc} = -K_{nc} \left[2M_6^i M_0^j + M_7^i M_{-1}^j + M_5^i M_1^j + A\lambda M_6^i M_{-1}^j + A\lambda M_5^i M_0^j \right. \\ \left. + A\lambda M_7^i M_{-2}^j + A\lambda M_4^i M_1^j \right]$$

$$\left. \frac{dM_0^j}{dt} \right|_{nc} = 0, \quad \left. \frac{dM_3^j}{dt} \right|_{nc} = - \left. \frac{dM_3^j}{dt} \right|_{nc}$$

$$\left. \frac{dM_6^j}{dt} \right|_{nc} = K_{nc} \left[2M_6^i M_0^j + M_7^i M_{-1}^j + M_5^i M_1^j + A\lambda M_6^i M_{-1}^j + A\lambda M_5^i M_0^j \right. \\ \left. + A\lambda M_7^i M_{-2}^j + A\lambda M_4^i M_1^j \right] + 2K_{nc} \left[2M_3^i M_3^j + M_4^i M_2^j + M_2^i M_4^j \right. \\ \left. + A\lambda M_3^i M_2^j + A\lambda M_2^i M_3^j + A\lambda M_4^i M_1^j + A\lambda M_1^i M_4^j \right]$$

(8)

where M_k^i indicates the k th moment of mode i . In the free-molecular regime, the equations can be written as

$$\left. \frac{dM_0^j}{dt} \right|_{fm} = -bK_{fm} \left[M_0^i M_{0.5}^j + M_{0.5}^i M_0^j + M_2^i M_{-1.5}^j + M_{-1.5}^i M_2^j + M_1^i M_{-0.5}^j + M_{-0.5}^i M_1^j \right]$$

$$\left. \frac{dM_3^j}{dt} \right|_{fm} = -bK_{fm} \left[M_3^i M_{0.5}^j + M_{3.5}^i M_0^j + M_5^i M_{-1.5}^j + M_{1.5}^i M_2^j + M_4^i M_{-0.5}^j + M_{2.5}^i M_1^j \right]$$

$$\left. \frac{dM_6^j}{dt} \right|_{fm} = -bK_{fm} \left[M_6^i M_{0.5}^j + M_{6.5}^i M_0^j + M_8^i M_{-1.5}^j + M_{4.5}^i M_2^j + M_7^i M_{-0.5}^j + M_{5.5}^i M_1^j \right]$$

$$\left. \frac{dM_0^j}{dt} \right|_{fm} = 0, \quad \left. \frac{dM_3^j}{dt} \right|_{fm} = - \left. \frac{dM_3^j}{dt} \right|_{fm}$$

Development of RAQM2 and Asian aerosol mixing type simulation

M. Kajino et al.

Title Page

Abstract

Introduction

Conclusions

References

Tables

Figures

◀

▶

◀

▶

Back

Close

Full Screen / Esc

Printer-friendly Version

Interactive Discussion



$$\left. \frac{dM_6^j}{dt} \right|_{\text{fm}} = bK_{\text{fm}} \left[M_6^i M_{0.5}^j + M_{6.5}^i M_0^j + M_8^i M_{-1.5}^j + M_{4.5}^i M_2^j + M_7^i M_{-0.5}^j + M_{5.5}^i M_1^j \right] + 2bK_{\text{fm}} \left[M_3^i M_{3.5}^j + M_{3.5}^i M_3^j + M_5^i M_{1.5}^j + M_{1.5}^i M_5^j + M_4^i M_{2.5}^j + M_{2.5}^i M_4^j \right] \quad (9)$$

where the approximation function b , newly proposed by Kajino (2011), is

$$b = 1 + 1.2\gamma \exp \left[-2 \frac{\sigma_i + \alpha \sigma_j}{1 + \alpha} \right] - 0.646\gamma \exp \left[-0.35 \frac{\sigma_i^2 + \alpha \sigma_j^2}{1 + \alpha} \right]$$

$$\gamma = \left[1 - \frac{\sqrt{1 + \alpha^3}}{1 + \sqrt{\alpha^3}} \right] / \left[1 - \frac{1}{\sqrt{2}} \right], \quad \alpha = \frac{D_{gj}}{D_{gi}} \quad (10)$$

The harmonic mean of the time derivative terms (Eq. 6) is applied to cover the full size range.

2.2.4 Number concentration of soot collided to coarse mode particles

Soot particles sometimes form internal mixture with coarse mode particles such as dust and sea salt particles, and such mixtures alter optical properties of the coarse mode particles significantly and contribute to atmospheric solar heating and surface dimming (Clarke et al., 2004; Zhu et al., 2007; Guazzotti et al., 2011). Such mixtures can be predicted in the RAQM2 model as BC mass and M_0^{AGR} number concentrations in the COR category (Table 2). M_0^{AGR} indicates the number concentration of soot particles (AGR) collided with COR particles and is calculated as

$$\frac{dM_0^{\text{AGR}}}{dt} = \left. \frac{dM_0}{dt} \right|_{\text{coag}}^{\text{COR-AGR}} \quad (11)$$

M_0^{AGR} exceeds the M_0 of COR because M_0^{AGR} does not indicate the number of COR particles internally mixed with soot but indicates the number of times each AGR particle hits COR particles. Brownian coagulation theory assumes the coalescence efficiency is unity, but it may not be true for the atmospheric aerosols. The efficiency of the bouncing/sticking of colliding atmospheric particles should be formulated.

2.2.5 Condensation

The zeroth moment $M_0 (= N)$ remains constant during the condensation process.

$$\frac{dM_0}{dt} = 0 \quad (12)$$

The condensational growth of the particle mass M of each category can be expressed as

$$\frac{dM}{dt} = \int \frac{m_{w,p}}{m_{w,g}} (c_\infty - c_s) \psi(d_p) n(d_p) dd_p \quad (13)$$

where $m_{w,p}$ and $m_{w,g}$ represent the molecular weights of semi-volatile components in the particle and gas phases, respectively, and c_∞ and c_s are the gas phase concentrations in the bulk phase (near the aerosol surface) and those on the aerosol surface, respectively. The ψ_s are different in the free-molecular and the near continuum regimes, which can be written as

$$\psi^{\text{fm}}(d_p) = \frac{\pi \alpha \bar{c}}{4} d_p^2 \quad (14a)$$

$$\psi^{\text{co}}(d_p) = 2\pi D_v d_p \quad (14b)$$

respectively, where α is a mass accommodation coefficient assumed constant as 0.1, \bar{c} is a mean velocity of the gas molecules, and D_v is the molecular diffusion coefficient.

Development of RAQM2 and Asian aerosol mixing type simulation

M. Kajino et al.

Title Page

Abstract

Introduction

Conclusions

References

Tables

Figures

⏪

⏩

◀

▶

Back

Close

Full Screen / Esc

Printer-friendly Version

Interactive Discussion



Using the harmonic mean approach to cover the two regimes, the time derivative term of arbitrary moments due to condensation can be rewritten as

$$\frac{dM_k}{dt} = \frac{dM}{dt} \frac{dM_k}{dM} = \frac{1}{\rho_p} \frac{m_{w,p}}{m_{w,g}} (c_\infty - c_s) \left| \frac{k\alpha\bar{c}}{2} M_{k-1}, 4kD_v M_{k-2} \right|_{\text{harm}} \quad (15)$$

where $|A, B|_{\text{harm}}$ indicates the harmonic mean of A and B and, thus, $AB/(A + B)$. The condensation growth of mass is expressed as

$$\frac{dM}{dt} = \frac{\pi\rho_p}{6} \frac{dM_3}{dt} \quad (16)$$

To obtain the gas phase concentrations on the aerosol surface c_s , which is thermodynamically equilibrated, ISORROPIA II (Fountoukis and Nenes, 2007) and Edney et al. (2007) are used for semi-volatile inorganic and organic compounds, respectively.

2.2.6 Simultaneous solution of nucleation, condensation and mode merging

RAQM2 achieved a completely dynamic (non-equilibrium) solution of a gas-to-particle mass transfer over a wide range of aerosol diameters from 1 nm to super-micrometer size. The new particle formation (NPF) process is, however, not dynamically solved, but parameterized, which is inevitable for the time and spatial scales of the simulation. Recently, numerous NPF parameterizations have been proposed based on laboratory experiments, theoretical and molecular dynamics calculations, and nanoparticle observations (Kulmala and Kerminen, 2008; Hirsikko et al., 2011). However, numerous uncertainties and discrepancies remain among each parameterization (Zhang et al., 2010). Therefore, we used the parameterizations based on several observations in diverse atmospheric locations (Kuang et al., 2008) to obtain the plausible nucleation rates for realistic conditions.

To solve the condensation onto the pre-existing particles and the nucleation of sulfuric acid gas, the operator and time splitting method was applied. The nucleation and

Development of RAQM2 and Asian aerosol mixing type simulation

M. Kajino et al.

Title Page

Abstract

Introduction

Conclusions

References

Tables

Figures

⏪

⏩

◀

▶

Back

Close

Full Screen / Esc

Printer-friendly Version

Interactive Discussion



condensation processes were solved simultaneously using the short split time step (Δt) of 1 s with an explicit method (forward in time) (see Sect. 2.2.9 and Fig. 2). We found that a 1-s time step was sufficient to yield an accurate nucleation rate under the realistic conditions of sulfuric acid gas up to 10^8 molecules (cm^{-3}) and aerosol number concentrations from 10^2 to 10^6 (cm^{-3}) using the Kuang et al. (2008) parameterization. When nucleation occurs, the number of new particles, produced within 1 s, with a D_g and σ of 1 nm and unity, respectively, were entered in the ATK category. Because the ATK particles swelled rapidly due to condensation and Brownian coagulations, the aerosols were merged to the larger particle category ACM, as shown in Table 3. The portion of the k th moment larger than a criteria diameter D_c were readily calculated using the error function $\text{erf}(x)$ as

$$[M_k]_{D_c} = \int_{\ln D_c}^{\infty} D^k n(\ln D) d \ln D = \frac{M_k}{2} \left[1 - \text{erf} \left(\frac{\ln D_c - \ln D_g - k \ln^2 \sigma}{\sqrt{2} \ln \sigma} \right) \right] \quad (17)$$

The portion of mass is identical to that of the third moment. Each moment and each mass of the chemical compositions in ATK exceeding D_c (set as 40 nm in the study) were merged into the ACM category using Eq. (17), and vice versa: when the shrinking of the ACM occurs, the portion of the moments and mass smaller than 40 nm are merged to ATK (Table 3).

2.2.7 Grid-scale and sub-grid-scale wet deposition

For the grid-scale wet deposition, the CCN activation and subsequent cloud microphysical processes were parameterized using Abdul-Razzak and Ghan (2000) and WSM6 (Lin et al., 1983). When the Abdul-Razzak and Ghan (2000) parameterization predicts that CCN activation occurs in a grid cell, the portions of the moments and the mass (see Eq. (17)) were transferred to the grid-scale cloud droplets. Lin et al. (1983) developed an explicit cloud microphysics model in which interactions between cloud droplets and

Development of RAQM2 and Asian aerosol mixing type simulation

M. Kajino et al.

Title Page

Abstract

Introduction

Conclusions

References

Tables

Figures

⏪

⏩

◀

▶

Back

Close

Full Screen / Esc

Printer-friendly Version

Interactive Discussion



Development of RAQM2 and Asian aerosol mixing type simulation

M. Kajino et al.

Title Page

Abstract

Introduction

Conclusions

References

Tables

Figures

⏪

⏩

◀

▶

Back

Close

Full Screen / Esc

Printer-friendly Version

Interactive Discussion

other hydrometers, such as rain, snow and graupel droplets, are formulated. The auto-conversion rate (cloud → rain) and the accretion rate of cloud droplets by rain, snow, and graupel (cloud → rain, cloud → snow, cloud → graupel), predicted by WSM6, were used to calculate the transfer of the aerosol moments and mass in the cloud droplets to the other hydrometers.

Particles such as hydrophobic forms of dust and soot efficiently act as IN in ice and mixed phase clouds. Pagels et al. (2009) found that a mass increase of 2–3 times by the condensation of water and sulfuric acid onto soot agglomerates resulted in a transformation to spherical shapes. We assumed here that the soot loses IN activity after the growth by condensation. Thus, hydrophobic particles in RAQM2 are defined as AGR and COR categories when the hygroscopic mass (= sum of SO_4^{2-} , NH_4^+ , NO_3^- , Cl^- and SS) is less than 50 % of the total dry mass, i.e., the hygroscopic mass is less than the hydrophobic mass (= sum of UIC, BC, OA and DU).

All components in OA were assumed to be hydrophobic here, although some of the secondary OA was hydrophilic. For the IN activation of aerosols, we used the parameterizations of Lohmann and Diehl (2010) for contact freezing and immersion (+ condensation) freezing. We assumed that the IN activation occurred only in a grid cell that contains ice particles predicted by WRF with a temperature lower than -3°C . The fractions of frozen droplets for dust and soot particles are assumed as functions of temperature based on Fig. 1 of Lohmann and Diehl (2010), respectively, as follows:

$$\begin{aligned}
 F_{\text{cn_du}} &= -14(T_c + 3) \\
 F_{\text{cn_bc}} &= -15(T_c + 10) \\
 F_{\text{im_du}} &= -0.1(T_c + 27) \\
 F_{\text{im_bc}} &= -0.5(T_c + 36)
 \end{aligned} \tag{18}$$

where $F_{\text{cn_du}}$, $F_{\text{cn_bc}}$, $F_{\text{im_du}}$, and $F_{\text{im_bc}}$ represent the fractions for the contact freezing of hydrophobic COR and AGR and the immersion freezing of hydrophobic COR and AGR, respectively, and T_c is the grid air temperature ($^\circ\text{C}$). For immersion freezing, the $F_{\text{im_du}}$ and $F_{\text{im_bc}}$ are the exact fractions scavenged into ice particles. For contact

freezing, some portion of $F_{\text{cn_du}}$ and $F_{\text{cn_bc}}$ actually coagulated with ice or super-cooled cloud droplets can be scavenged into ice particles. The Brownian coagulation of hydrophobic COR and AGR with cloud ice/water droplets was calculated using the inter-category coagulation Eqs. (6), (8), (9) and (10). To obtain the size distribution of cloud ice/water droplets, we assumed a simple Khrgian-Mazin-type gamma size distribution (Pruppacher and Klett, 1997):

$$n(a) = Aa^2 \exp(-Ba) \quad (19)$$

where $n(a)$ is the number size distribution function, A and B are parameters related to moments of the distribution, and a is a particle radius. This Khrgian-Mazin equation is almost identical to the LNSD, with a standard deviation of approximately 1.64. Thus, assuming a D_g of cloud ice/water droplets of $15 \mu\text{m}$ together with cloud ice/water mixing ratios and their density, the size distribution can be fixed for the intercategory Brownian coagulation. Subsequently, aerosols in ice particles are converted to snow via autoconversion (aggregation) and are converted to rain, snow and graupel particles due to accretion, with conversion rates predicted by the explicit cloud microphysics parameterization (WSM6).

The below-cloud scavenging process is considered inter-category coagulation with falling hydrometers, such as rain, snow and graupel droplets. Kajino and Kondo (2011) deduced the collision/coalescence equations due to gravitational settling in Eqs. (A37)–(A43) in section A.4 of their paper. The LNSD is assumed in their equations, while the size distributions of such hydrometers are often represented by a gamma function. Thus, we first derive the gamma size distributions (GSDs) of the hydrometers as a function of the mixing ratio (Hong and Lin, 2006) and then yield the LNSD converted from GSD, preserving the three moments.

Once captured in the hydrometeors in either ways, a certain portion of the moments and chemical components is assumed to immediately reach the ground in the same manner as Eqs.(1) and (2) in Kajino and Kondo (2011).

Development of RAQM2 and Asian aerosol mixing type simulation

M. Kajino et al.

Title Page

Abstract

Introduction

Conclusions

References

Tables

Figures

⏪

⏩

◀

▶

Back

Close

Full Screen / Esc

Printer-friendly Version

Interactive Discussion

2.2.8 Dry deposition and gravitational sedimentation

The dry deposition and gravitational sedimentation processes are formulated in the same manner as that given in Appendices 5 and 6 of Kajino and Kondo (2011) through Eqs. (A44) to (A48). With regard to the calculation of dry deposition for particles, however, the original parameterization of surface resistance by Zhang et al. (2001) used in Kajino and Kondo (2011) was modified based on comparisons using observational data by more recent works (Katata et al., 2008, 2011; Petroff and Zhang 2010) to improve the prediction accuracy of dry deposition. In the present paper, four important revisions were performed:

1. On the assumption that forests have tall canopies and a large leaf surface area that enables a large amount of particles from the atmosphere to be captured, the empirical constant ε_0 in Zhang et al. (2001) was set to 5 and 1 for the categories of forest and short vegetation, respectively. This modification decreases the surface resistance, resulting in large values of dry deposition velocity for forest compared with other vegetation.
2. For the collection efficiency by leaves due to inertial impaction, the modified function of Peters and Eiden (1992) (Eq. (7) in Katata et al., 2008) was used. The function was validated with the data of fog deposition ($> 1 \mu\text{m}$) onto coniferous and broad-leaved forests in Katata et al. (2008).
3. Collection efficiencies due to interception and Brownian diffusion by Kirsch and Fuchs (1968) and Fuchs (1964) (Eqs. (14) and (16) in Katata et al., 2011), respectively, were also used for vegetative surfaces. Those formulations were verified using the flux data of fine aerosols ($< 1 \mu\text{m}$) over the coniferous forest in Katata et al. (2011).
4. For the land use categories of desert, tundra, ice cap and glacier, inland water, and ocean, the surface resistance for non-vegetated surfaces proposed by Petroff and Zhang (2010) were adopted.

Development of RAQM2 and Asian aerosol mixing type simulation

M. Kajino et al.

Title Page

Abstract

Introduction

Conclusions

References

Tables

Figures

⏪

⏩

◀

▶

Back

Close

Full Screen / Esc

Printer-friendly Version

Interactive Discussion



Development of RAQM2 and Asian aerosol mixing type simulation

M. Kajino et al.

Title Page

Abstract

Introduction

Conclusions

References

Tables

Figures

⏪

⏩

◀

▶

Back

Close

Full Screen / Esc

Printer-friendly Version

Interactive Discussion



After the above modifications, the dry deposition velocity calculated by the modified model agreed better with the observational data than the original model of Zhang et al. (2001). For example, the size-segregated dry deposition velocity for the vegetative surface decreased and increased by one order of magnitude within a 0.1- and 1- μm -diameter range, which is comparable to the performance of the detailed multi-layer particle deposition model by Katata et al. (2011). For ground and water surfaces, a good agreement between calculations by the modified model and observations from the literature was found, as shown in Petroff and Zhang (2010).

2.2.9 Operator splitting and time splitting for aerosol dynamical modeling

The operator splitting and time splitting used for the aerosol dynamics module are illustrated in Fig. 2. In the flow chart, each solid box indicates each operator, and the arrows denote the order of operator calculations. ΔT_{host} is the longest time step of the host calculation, i.e., horizontal advection and diffusion. In this study, we set $\Delta x = 60\text{ km}$, so ΔT_{host} is set as 300 s after optimization of the CPU time and the deficit of numerical diffusions. Δt is a split time step within each operator calculation, whereas the ΔT s denote the integrated time steps of each operator before stepping forward to the next operator. First, the production rate of sulfuric acid gas via homogeneous (gas phase) chemistry was calculated using SAPRC99 with the Eulerian Backward Iteration method with $\Delta t = 150\text{ s}$. The production rate of sulfuric acid gas was obtained as $\Delta C_{\text{H}_2\text{SO}_4} / \Delta T_{\text{host}}$. The nucleation rate $J_{1\text{nm}}$ (Kuang et al., 2008) and the condensation rate (Eqs. 15 and 16) were calculated using $C_{\text{H}_2\text{SO}_4} = \Delta C_{\text{H}_2\text{SO}_4} / \Delta T_{\text{host}} \times \Delta t (= 1\text{ s})$. Then, the gas-phase concentration $C_{\text{H}_2\text{SO}_4}$ was distributed into the ATK category to produce new particles and into all categories by condensation simultaneously. After finishing the NPF&Cond. operator, the intra-category and inter-category Brownian coagulation was solved with an arbitrary split time to integrate for $0.5\Delta T_{\text{host}}$ (150 s). CFL-like conditions

were established for Brownian coagulation as

$$t_{\text{CFL}} = M_0^i / \frac{dM_0^i}{dt} \quad (20)$$

where Δt is set as the maximum so that it never exceeds $0.5 \times t_{\text{CFL}}$ for all the categories due to intra- and inter-category coagulations. After the Coag. operator is calculated for half the host time step, the condensation of the semi-volatile inorganic and organic components is calculated. The CFL conditions are also introduced for the condensation process as

$$t_{\text{CFL}} = 1/k_w \quad (21)$$

where k_w is the mass-transfer coefficient (s^{-1}) for each category defined as

$$k_w = \frac{dM}{dt} \frac{1}{(c_\infty - c_s)} \quad (22)$$

and the time derivative of mass concentration dM/dt is obtained from Eqs. (15) and (16). Δt is set as the maximum so that it never exceeds $0.1 \times t_{\text{CFL}}$ for all categories. The condensation process was integrated for the host time step period (300 s) with the arbitrary time step. After the volatile components condensation operator, the Coag. operator was calculated again for the remaining half of the host time step (150 s). Other processes then follow, including sedimentation, dry deposition, subgrid-scale convection and wet deposition, grid-scale CCN activation and cloud microphysics.

Strictly speaking, NPF, the condensation of sulfuric acid gas and other semi-volatile components, and Brownian coagulation should be solved with the smallest time step, i.e., 1 s, to calculate the growth of aerosol particles consistently. However, although ISORROPIA2 is computationally efficient compared with other models (Fountoukis and Nenes, 2007), solving the thermodynamic equilibrium state among multi-component species for every 1 s for all categories in the regional scale simulation is still far from

Development of RAQM2 and Asian aerosol mixing type simulation

M. Kajino et al.

Title Page

Abstract

Introduction

Conclusions

References

Tables

Figures

⏪

⏩

◀

▶

Back

Close

Full Screen / Esc

Printer-friendly Version

Interactive Discussion



feasible for our computational resources. Therefore, $\Delta T_{\text{Cond.}}$ is set equal to ΔT_{host} , but ΔT of the Brownian coagulation operator is divided in two ($\Delta T_{\text{Coag.}} = 0.5\Delta T_{\text{host}}$) and inserted separately before and after the condensational operator in the current implementation of the model (Fig. 2).

3 Model evaluation using observation data

3.1 EANET monitoring network data

Acid Deposition Monitoring Network in East Asia (EANET) data were used for model evaluation. The guidelines, technical documents, monitoring reports and quality assurance and quality control programs are available at <http://www.eanet.cc/product.html>. We used hourly SO_2 , NO_x , O_3 , $\text{PM}_{2.5}$ and PM_{10} concentrations and meteorological parameters, and 1- or 2- weekly concentrations of gases (SO_2 , NH_3 , HNO_3 , and HCl) and aerosols components (SO_4^{2-} , NO_3^- , Cl^- , NH_4^+ , Na^+ , Mg^{2+} , K^+ , and Ca^{2+}) using the filter pack method (FP). The long-duration sampling of FP causes several artifact problems; volatilization of NH_4NO_3 and NH_4Cl collected on a filter occur during sampling and/or high humidity may reduce measured gas concentration due to trapping by condensed water in the filter pack. To avoid the problems, only total nitrate (T-NO_3^- ; HNO_3^- gas plus NO_3^- aerosol), total ammonium (T-NH_4^+ ; NH_3 gas plus NH_4^+ aerosol), and total chloride (T-Cl^- ; HCl gas plus Cl^- aerosol) are used for in this study.

To obtain the anthropogenic SO_4^{2-} and Ca^{2+} originating from the Asian dust (calcite), nss-SO_4^{2-} and nss-Ca^{2+} were defined, excluding the contribution of sea salt using a standard mean chemical composition of sea water (DOE, 1994), as follows:

$$[\text{nss-SO}_4^{2-}] = [\text{SO}_4^{2-}] - 0.251 \times [\text{Na}^+] \quad (23)$$

$$[\text{nss-Ca}^{2+}] = [\text{Ca}^{2+}] - 0.038 \times [\text{Na}^+] \quad (24)$$

where [] denotes the weight concentrations in $\mu\text{g m}^{-3}$.

Development of RAQM2 and Asian aerosol mixing type simulation

M. Kajino et al.

Title Page

Abstract

Introduction

Conclusions

References

Tables

Figures

⏪

⏩

◀

▶

Back

Close

Full Screen / Esc

Printer-friendly Version

Interactive Discussion



Development of RAQM2 and Asian aerosol mixing type simulation

M. Kajino et al.

Title Page

Abstract

Introduction

Conclusions

References

Tables

Figures

⏪

⏩

◀

▶

Back

Close

Full Screen / Esc

Printer-friendly Version

Interactive Discussion



Among the EANET stations, six stations in Japan are selected for the model evaluation, as depicted in Fig. 1 and listed in Table 4. The red triangles denote the stations located on small islands or isolated capes in down-wind regions. These stations were situated in areas without nearby large anthropogenic emission sources and without the complexity of local orographic winds; therefore, high concentration episodes mostly coincided with synoptic-scale disturbances and were well simulated by regional-scale models. On the other hand, because those stations were very close to ocean surfaces, the regional-scale simulations of ocean-originated species such as sea salt did not often agree well with the observations. We often obtained a better agreement for sea salt-originated components at inland or mountainous stations.

3.2 Q-AMS aerosol observation data at the CHAAMS site

Because the temporal resolution of the ionic aerosol component measurements of EANET is 2 weeks, the simulated transport and transformation of aerosol components cannot be evaluated. Alternatively, we used the hourly concentrations of $\text{PM}_{1\text{-nss}}\text{-SO}_4^{2-}$, $\text{PM}_{1\text{-nss}}\text{-NO}_3^-$, $\text{PM}_{1\text{-nss}}\text{-Cl}^-$, and $\text{PM}_{1\text{-nss}}\text{-NH}_4^+$ (50 % cutoff of aerosols with an aerodynamic diameter of $1\ \mu\text{m}$), measured using a quadrupole aerosol mass spectrometer (Aerodyne Research Inc., Q-AMS) at the Cape Hedo Atmospheric and Aerosol Monitoring Station (CHAAMS) site (Takami et al., 2007; Takiguchi et al., 2008). The CHAAMS site is located within the same premises as the EANET Hedo station.

3.3 Bulk mass concentrations of gaseous species

It was necessary to predict the O_3 concentration precisely because it is an important oxidizing agent in the atmosphere for secondary aerosol formations. This prediction was also important because O_3 is a source of the most efficient oxidants in the troposphere, OH radicals. Because O_3 is a relatively longer-lived species, the contribution of inter-continental transport and stratospheric ozone intrusion is substantial (Sudo and Akimoto, 2007; Nagashima et al., 2010). Consequently, the seasonal trends can

never be reproduced by a tropospheric regional-scale model itself without appropriate seasonal variations of the lateral and upper (tropopause) boundary conditions. Therefore, we used the climatological simulation results of monthly NO_x , O_x , CO and VOCs concentrations using a global-scale stratospheric and tropospheric chemistry-climate model (MRI-CCM2; Deushi and Shibata, 2011) as the boundary conditions of RAQM2.

Table 5 summarizes the statistical analysis for the comparison between the observation and simulation of all the available data at the six EANET stations. The simulation of daily maximum 8-h mean O_3 was found to be successful, as the medians of observation and simulation were close to each other and the Root Mean Square Errors (RMSEs) were much lower than the medians. The correlation coefficient R is 0.47 and 96 % of the data-satisfied factor of 2. The R of the daily mean SO_2 and NO_x concentrations was the same as that of O_3 , whereas there were larger discrepancies in the medians, RMSEs, FAC2 and FAC5. Because these EANET stations are located over remote ocean areas, the temporal variations of O_3 were always incremented by background concentrations due to the long-range transport. While this smaller variation/background ratio of O_3 resulted in better scores for RMSEs, FAC2 and FAC5 than SO_2 and NO_x , the same levels of R indicate that the predictability of the transport patterns of the three species were similar. The simulated O_3 was not biased toward the observation, but the simulated SO_2 and NO_x were biased by 30–50 %.

3.4 Bulk mass concentrations of aerosol chemical components

Fig. 3 presents a scatter diagram between the observed and modeled concentrations of biweekly chemical components at the Rishiri, Oki and Hedo stations. These stations are located over a wide range, from the northeast to the southwest of the Japan archipelago, so different types of long-range transport patterns from the Asian continent can be evaluated. We also selected these stations because the $\text{PM}_{2.5}$ mass concentrations were monitored together with PM_{10} only at Rishiri and Oki and because the AMS PM_1 measurements were taken only at Hedo.

Development of RAQM2 and Asian aerosol mixing type simulation

M. Kajino et al.

Title Page

Abstract

Introduction

Conclusions

References

Tables

Figures

⏪

⏩

◀

▶

Back

Close

Full Screen / Esc

Printer-friendly Version

Interactive Discussion



Development of RAQM2 and Asian aerosol mixing type simulation

M. Kajino et al.

Title Page

Abstract

Introduction

Conclusions

References

Tables

Figures

⏪

⏩

◀

▶

Back

Close

Full Screen / Esc

Printer-friendly Version

Interactive Discussion

The statistics of the corresponding data at all six stations are listed in Table 5. The medians of the modeled nss-SO_4^{2-} and T-NH_4^+ were approximately 30 % smaller than the observed, whereas the modeled T-NO_3^- was almost double that observed. The nitric acid and ammonia are semi-volatile in atmospheric conditions and were partitioned into gas and aerosol phases. However, due to the artifact problems mentioned in Sect. 3.1, the gas-aerosol partitioning was not evaluated. The partitioning is essentially important for the transport of the species because the dry and wet deposition efficiencies of nitric acid and ammonia in gas and aerosol phases are very different (Kajino et al., 2008). The modeled gas-aerosol partitioning of the semi-volatile components should be evaluated using accurate measurements for HNO_3 and NH_3 gases in the future to identify the possible causes of the discrepancies between the model and observation. The RMSEs of nss-SO_4^{2-} , NH_4^+ , and NO_3^- were comparable to the medians, and the R^2 values were always greater than 0.5.

T-Cl^- and Na^+ mainly originate from sea salt particles because the EANET stations are close to the ocean. Natural aerosols are usually difficult to simulate due to the large uncertainties in the emission flux estimations, and the R_s were lower than the other chemical components. Still, the RMSEs and modeled medians were close to the observed medians. nss-Ca^{2+} was considered to originate from Asian dust particles, which contain calcite; these are also natural aerosols and were difficult to simulate. The modeled median was approximately double that measured. We assumed uniform compositions for dust emission from the whole model domain, which may not have been natural. Still, a large value of R was obtained for nss-Ca^{2+} because the long-range transport of Asian dust in Japan is most influential in spring, and this feature was well reproduced by RAQM2. The R_s at the Western stations, where the dust transport is more frequent, were especially larger, with 0.74 and 0.76 at Hedo and Oki, respectively.

3.5 Size distributions of total aerosol mass

Fig. 4 presents the daily mean observed and modeled concentrations of PM_{10} , $\text{PM}_{2.5}$, and $\text{PM}_{2.5}/\text{PM}_{10}$ concentration ratios and modeled constituent fractions of PM_{10} , $\text{PM}_{2.5}$,

Development of RAQM2 and Asian aerosol mixing type simulation

M. Kajino et al.

Title Page

Abstract

Introduction

Conclusions

References

Tables

Figures

⏪

⏩

◀

▶

Back

Close

Full Screen / Esc

Printer-friendly Version

Interactive Discussion

and PM_{10} at the Rishiri and Oki stations. $PM_{2.5}$ includes sub-micron aerosols and a portion of super-micron aerosols, such as sea salt and dust particles, so the $PM_{2.5}/PM_{10}$ ratio provided some idea of the mass size distribution of the super-micron particles or mass ratios of anthropogenic (mostly sub-micron) and natural origin aerosols (mostly super-micron) (Kajino and Kondo, 2011). Notably, the modeled $PM_{2.5}$ and PM_{10} were derived using Eq. (17) by cutting each wet aerosol category at the exact diameter (2.5 and 10 μm , respectively), so the size classification property differed from that of the instruments, characterized by the so-called cut-off curve. As shown in Table 5, the medians of the modeled $PM_{2.5}$ and PM_{10} are 40 % and 50 % smaller, respectively, than the observed. The RMSEs were comparable to the median values, and approximately half of the data satisfied a factor of 2 and more than 80 % satisfied a factor of 5. Notably, the statistics for PM_{10} included data from all six stations, whereas those for $PM_{2.5}$ included only those from Oki and Rishiri. The modeled and observed median of the $PM_{2.5}/PM_{10}$ ratio agreed well, as the RMSE is small and more than 80 % of the data satisfied a factor of 2, except that R is almost zero. Together with the comparison shown in Fig. 4e,f, the daily variations of the $PM_{2.5}/PM_{10}$ ratio may have failed to be simulated, but longer-term features were well reproduced by the model. The variations of the measured ratios were not large, with the median ranging from 0.4 to 0.6. The values at Oki (0.9) in August were excluded because the measured $PM_{2.5}$ data were missing during most of the period. The modeled mean $PM_{2.5}/PM_{10}$ ratios were also within the same range of 0.4–0.6, except at Rishiri from January to March. The overestimation of the model during the period indicates that the modeled size was smaller than that observed.

The 10-d mean fractions of the PM_{10} , $PM_{2.5}$, and PM_{10} constituents are also shown in Fig. 4g–i. The red, green, yellow, blue, and sky blue columns indicate the total dry mass of ATK and ACM, the total dry mass of AGR, the dust mass (DU) of COR, the sea salt mass ($SS + Cl^-$) of COR, and the other dry mass of COR, respectively. The ATK, ACM, and AGR are mainly of anthropogenic origin and are composed of submicron particles (PM_{10}). COR is mainly of natural origin and was partitioned into $PM_{2.5}$ and PM_{10} . The ATK, ACM, and AGR particles accounted for more than 90 % of the PM_{10} except in

spring and autumn at Rishiri and spring at Oki. The COR particles accounted for more than 90 % of the PM_{10} except in summer. The modeled fractions of ATK, ACM, and AGR in $PM_{2.5}$ and PM_{10} became larger in summer because the sea salt production and dust transport are less pronounced than those in the cold seasons. The $PM_{2.5}/PM_{10}$ ratio of the chemical components was an excellent indicator of the mixing type of the inorganic components (Kajino and Kondo, 2011), but that of the total aerosol mass was merely an indicator of the COR category sizes. The modeled fractions of the constituents of $PM_{2.5}$ and PM_{10} did not differ greatly from one another, but those of PM_1 and PM_{10} were very different. Unfortunately, we did not obtain PM_1 mass concentration data, but a comparison between the modeled and observed PM_1/PM_{10} ratio, if available, may provide additional important implications for modeling studies.

3.6 Size distributions and mixing types of inorganic components

Figure 5 shows the observed and modeled (left) daily mean PM_1 concentrations of the $nss-SO_4^{2-}$, NH_4^+ , NO_3^- , and Cl^- concentrations and (right) the biweekly mean bulk concentrations of $nss-SO_4^{2-}$, $T-NH_4^+$, $T-NO_3^-$, $T-Cl^-$, Na^+ , and $nss-Ca^{2+}$. To derive the modeled PM_1 concentrations for the comparisons with the AMS data, Eq. (17) was again applied. Notably, the equation was applied for the modeled “dry” size distribution, whereas it was applied for the “wet” size distribution for the cases of $PM_{2.5}$ and PM_{10} , corresponding to the measurement techniques.

Table 6 summarizes the statistical analysis of the corresponding data shown in Fig. 5. In summer, the Pacific high is influential, carrying a clean maritime air mass to Hedo. In cold seasons, long-range transport from the Asian continent via cyclonic fronts or anticyclones propagating eastward is predominant. Therefore, the concentrations of air pollutants are low in summer and high in spring, autumn, and winter. These seasonal features and daily variations were successfully reproduced by the model. The model results of the natural aerosols, such as sea salt (Na^+) and Asian dust (Ca^{2+}), at Hedo

Development of RAQM2 and Asian aerosol mixing type simulation

M. Kajino et al.

Title Page

Abstract

Introduction

Conclusions

References

Tables

Figures

⏪

⏩

◀

▶

Back

Close

Full Screen / Esc

Printer-friendly Version

Interactive Discussion



were also successful. The transport events of the Asian dust in spring and autumn were found in both the observation and simulation.

Although the variations were well simulated, the levels were underestimated for some components, such as $\text{PM}_1\text{-nss-SO}_4^{2-}$ and $\text{PM}_1\text{-NH}_4^+$. The modeled medians were approximately 30 % of those observed (Table 6). The model also underestimated the bulk nss-SO_4^{2-} and T-NH_4^+ , and the underestimation was consistent with that for PM_1 . The underestimations of $\text{PM}_1\text{-nss-SO}_4^{2-}$ and $\text{PM}_1\text{-NH}_4^+$ were most likely due to the underestimation of the bulk mass. The trends and values of $\text{PM}_1\text{-NO}_3^-$ were well predicted by the model, whereas the T-NO_3^- was overestimated.

Figure 6 presents the (left) biweekly mean PM_1 to the total (gas plus aerosol) concentration ratios for nss-SO_4^{2-} , T-NH_4^+ , T-NO_3^- , and T-Cl^- . The observed values were depicted only when the available hourly AMS data exceeded 50 % during each biweekly FP period (more than 140 hourly data out of the two weeks). The statistical values between the observed and modeled data are listed in Table 6. Figure 6 also presents (right) the biweekly mean fractions of gas and aerosol categories for each inorganic component. The observed median of the PM_1 to bulk nss-SO_4^{2-} ratio was 0.85. The ratio exceeded 1.0 for some cases, so it may be within the uncertainties of the analysis (Fig. 6a). The modeled ratio was also large because approximately 80 % of the nss-SO_4^{2-} was mixed with submicron particles, such as ATK, ACM and AGR (Fig. 6b). The modeled median was 0.66, which was smaller than that observed, indicating that the modeled size distribution of nss-SO_4^{2-} may have been larger than that observed or may indicate that the proportions mixed with larger COR particles might have been overestimated. The features of the NH_4^+ ratio were similar to those for nss-SO_4^{2-} because nss-SO_4^{2-} is a major counterpart of NH_4^+ . A range of 20–60 % of T-NH_4^+ existed in the gas phase in summer as NH_3 because the temperature was high enough for NH_4NO_3 to evaporate and/or the amount of nss-SO_4^{2-} was not enough to consume NH_3 gas to fix it to the aerosol phase as ammonium sulfate. Because the modeled nss-SO_4^{2-}

Development of RAQM2 and Asian aerosol mixing type simulation

M. Kajino et al.

Title Page

Abstract

Introduction

Conclusions

References

Tables

Figures

⏪

⏩

◀

▶

Back

Close

Full Screen / Esc

Printer-friendly Version

Interactive Discussion



SO_4^{2-} and NH_4^+ were both underestimated, the improvement of nss-SO_4^{2-} could also result in the improvement of NH_4^+ .

The seasonal trends of the mixing type of nss-SO_4^{2-} were interesting. nss-SO_4^{2-} internally mixed with ATK + ACM was the greatest in summer (June to July). Because the air is cleaner in summer, there are fewer surface areas of pre-existing aerosols for H_2SO_4 gas to condense onto, and new particle formation would occur more frequently. In contrast, in cold seasons, due to the abundance of preexisting aerosols including soot, H_2SO_4 gas was efficiently condensed onto the soot particles (AGR). However, the current analysis could not prove the plausibility of the mixing type. For this proof, the results should be evaluated in the future by comparing them with the measurements of the soot mixing state using a Volatility Tandem Differential Mobility Analyzer (VTDMA), a Single Particle Soot Photometer (SP2), or a Transmission Electron Microscope (TEM). The modeled nss-SO_4^{2-} was mixed with COR from 10–40%. The crustal components in COR, such as Na^+ in sea-salt or Ca^{2+} in Asian dust, could be counterparts of nss-SO_4^{2-} . The proportions show maxima in spring from March to May (40% in April as a maximum), which coincides with the Asian dust transport period at Hedo (Fig. 5j). In the current setting of RAQM2, unfortunately, the dust particles are categorized as COR together with sea salt particles, so we cannot evaluate nss-SO_4^{2-} mixed solely with Asian dust. Because the modeled nss-SO_4^{2-} was mixed with COR, either with sea salt or Asian dust throughout the year, the modeled PM_1 to bulk ratio was approximately 0.6. The observed ratio also sometimes dropped to the modeled levels, even less than half in May. Although certain discrepancies remained between the modeled and observed ratios, the modeled partitioning may not be so far from reality.

The mixing type of NO_3^- at Hedo was interesting when it was compared with that at Gosan, Jeju Island, Korea (shown in Fig. 1). The observed and modeled medians of the PM_1 to T-NO_3^- ratios were 0.054 and 0.035, respectively, more than 1 order of magnitude smaller than those for nss-SO_4^{2-} and NH_4^+ . This result means that the observed and modeled T-NO_3^- partitioned into the gas phase or internally mixed with

Development of RAQM2 and Asian aerosol mixing type simulation

M. Kajino et al.

Title Page

Abstract

Introduction

Conclusions

References

Tables

Figures

⏪

⏩

◀

▶

Back

Close

Full Screen / Esc

Printer-friendly Version

Interactive Discussion

Hedo, whereas approximately 50 % is mixed with sea salt over the Yellow Sea, where Gosan is located (Fig. 6l of Kajino and Kondo, 2011).

The mixing type of NO_3^- may be important for the size distribution of aerosols and its light scattering property. Although the same amounts of aerosol NO_3^- existed in the air, HNO_3 condensed onto submicron particles forming NH_4NO_3 , together with its water uptake, enhances the particle size efficiently and alter the light scattering property. However, HNO_3 condensed onto sea salt particles may not alter the particle size and optical property as significantly. It is because it expels HCl at the same time, the water uptake property may not change much, and the size increase ratio will be smaller than that for submicron particles as the sea salt particles are much larger.

The observed and modeled medians of the PM_{10} to T-Cl^- ratios were one order of magnitude smaller than those for T-NO_3^- . Almost all (99.4 % on average) of the aerosol phase Cl^- was mixed with COR particles. The modeled fractions of HCl gas showed a maximum in summer, with a value of 51 %. Because anthropogenic HCl emission was not considered in the current settings of RAQM2, the modeled T-Cl^- are all of sea salt origin. The temperature is high and the air is photochemically active in summer, so the HNO_3 gas concentration is also high. HNO_3 gas efficiently condensed onto sea-salt particles and expelled the Cl^- into the gas phase by the chlorine deficit reaction (Eq. 28) in summer.

4 Conclusions

A new aerosol chemical transport model, Regional Air Quality Model 2 (RAQM2), was developed to simulate Asian air quality. We implemented a simple version of a modal-moment aerosol dynamics model (MADMS; Kajino 2011) and achieved a completely dynamic (non-equilibrium) solution of a gas-to-particle mass transfer over a wide range of aerosol diameters, from 1 nm to super μm . The MADMS model is unique because it can solve inter-modal coagulation between two modes with very different log-normal size parameters. To consider a variety of atmospheric aerosol properties, the category

Development of RAQM2 and Asian aerosol mixing type simulation

M. Kajino et al.

Title Page

Abstract

Introduction

Conclusions

References

Tables

Figures

⏪

⏩

◀

▶

Back

Close

Full Screen / Esc

Printer-friendly Version

Interactive Discussion



Development of RAQM2 and Asian aerosol mixing type simulation

M. Kajino et al.

Title Page

Abstract

Introduction

Conclusions

References

Tables

Figures

⏪

⏩

◀

▶

Back

Close

Full Screen / Esc

Printer-friendly Version

Interactive Discussion

approach of EMTACS (Kajino and Kondo, 2011) is utilized. In RAQM2, aerosols are distributed into 4 categories: (1) Aitken mode (ATK), (2) soot-free accumulation mode (ACM), (3) soot aggregates (AGR) and (4) coarse mode (COR). New particle formation, condensation/evaporation, and intra/inter category coagulations for each category are solved dynamically. A regional-scale simulation ($\Delta x = 60\text{ km}$) was performed for the entire year of 2006 covering the northeast Asian region.

To evaluate the model performance on the major inorganic components in the air, we used observed hourly air concentrations of SO_2 , NO_x , O_3 , $\text{PM}_{2.5}$, and PM_{10} . We also used 1- or 2-weekly air concentrations of aerosol nss-SO_4^{2-} , total (gas plus aerosol) (T)- NO_3^- , T- Cl^- , T- NH_4^+ , Na^+ , and nss-Ca^{2+} of the Acid Deposition Monitoring Network in East Asia (EANET). Higher temporal-resolution data of aerosol components were used, and the hourly concentrations of $\text{PM}_1\text{-nss-SO}_4^{2-}$, $\text{PM}_1\text{-NO}_3^-$, $\text{PM}_1\text{-Cl}^-$, and $\text{PM}_1\text{-NH}_4^+$ were measured using a quadrupole aerosol mass spectrometer (Aerodyne Research Inc., Q-AMS) at the Cape Hedo Atmospheric and Aerosol Monitoring Station (CHAAMS).

Statistical analyses showed that the model reproduced the regional-scale transport and transformation of the major inorganic anthropogenic and natural air constituents within factors of 2 to 5. The modeled size distributions ($\text{PM}_{2.5}/\text{PM}_{10}$ and PM_1/bulk ratios) of the total weight and chemical components were assessed. We concluded that our prediction of aerosol mixing types (ATK, ACM, AGR and COR) of inorganic aerosol components such as nss-SO_4^{2-} , NH_4^+ , NO_3^- , and Cl^- were successful.

The modeled mixing types of the chemical components were found to be interesting. The Nss-SO_4^{2-} internally mixed with ATK + ACM was greatest in summer (June to July). Because the air is cleaner in summer, there are less surface areas of preexisting aerosols for H_2SO_4 gas to condense onto; thus, new particle formation would occur more frequently. In contrast, in cold seasons, due to the abundance of preexisting aerosols including soot, H_2SO_4 gas was efficiently condensed onto the soot particles (AGR). To evaluate the results, the modeled mixing type should be evaluated in the future by comparing it with measurements of the soot mixing state

using Volatility Tandem Differential Mobility Analyzer (VTDMA), Single Particle Soot Photometer (SP2), or Transmission Electron Microscope (TEM) analysis.

The difference in mixing type of the NO_3^- at Hedo and Gosan was interesting. Ninety-eight percent of the modeled NO_3^- was internally mixed with COR at Hedo, whereas 53.7% of the NO_3^- was internally mixed with sea salt particles at Gosan (Kajino and Kondo, 2011). The modeled values were consistent with the observed $\text{PM}_{2.5}/\text{PM}_{10}$ ratio of the NO_3^- at Gosan and the $\text{PM}_1/\text{T-NO}_3^-$ ratio at Hedo. Gosan is located upwind of Hedo toward the Asian continent. To the downwind regions of the continent over the ocean, the HNO_3 gas produced during transport is more efficiently condensed onto sea salt particles, as the proportions of the sea salt surface area to the total aerosol surface area become large. The chlorine deficit reaction on the sea salt particles promoted the condensation of HNO_3 . This reaction decreases HNO_3 gas concentration, resulting in evaporation of NH_4NO_3 from submicron particles. This conversion of nitrate in submicron particles to sea salt particles might occur during transport.

The aerosol mixing types presented in this study are key parameters for the light-scattering and absorbing properties. Further investigation is needed by comparing the results with aerosol optical thickness (AOT) or single scattering albedo (SSA) observations for the accurate assessment of aerosol-radiation interaction processes.

Acknowledgements. This research was promoted by the Fundamental Research Budget of the Meteorological Research Institute of Japan, "Studies on Atmospheric Aerosol Properties and Processes". The study was partly supported by the Environment Research and Technology Development Fund (Project No. B-0905 and A-1101) of the Ministry of the Environment of Japan and the Ministry of Education, Science, Sports and Culture (MEXT) Grant-in-Aid for Scientific Research (B), 23310018, 2011. Special thanks are due to G. Katata of the Japan Atmos Energy Agency (JAEA) for discussion on the dry deposition parameterizations of the gas and aerosols.

Development of RAQM2 and Asian aerosol mixing type simulation

M. Kajino et al.

Title Page

Abstract

Introduction

Conclusions

References

Tables

Figures

⏪

⏩

◀

▶

Back

Close

Full Screen / Esc

Printer-friendly Version

Interactive Discussion



References

- Abdul-Razzak, H. and Ghan, S. J.: A parameterization of aerosol activation. 2. Multiple aerosol types, *J. Geophys. Res.*, 105(D5), 6837–6844, 2000.
- An, J., Ueda, H., Wang, Z., Matsuda, K., Kajino, M., and Cheng, X.: Simulations of monthly mean nitrate concentrations in precipitation, *Atmos. Environ.*, 36, 4159–4171, 2002.
- An, J., Ueda, H., Matsuda, K. Hasome, H., and Iwata, M.: Simulated impacts of SO₂ emissions from the Miyake volcano on concentration and deposition of sulfur oxides in September and October of 2000, *Atmos. Environ.*, 37, 3039–3046, 2003.
- Binkowski, F. S. and Shankar, U.: The regional particulate model: 1. Model description and preliminary results, *J. Geophys. Res.*, 100, 26191–26209, doi:10.1029/95JD02093, 1995.
- Byun, D. and Schere, K. L.: Review of the governing equations, computational algorithms, and other components of the Models-3 Community Multiscale Air Quality (CMAQ) Modeling System, *Appl. Mech. Rev.*, 59, 51–77, 2006.
- Carter, W.: Documentation of the SAPRC-99 chemical mechanism for VOC reactivity assessment. Final report to California Air Resources Board, Rep. 92–329, Univ. of Calif., Riverside, 8 May, 2000.
- Carlton, A. G., Turpin, B. J., Altieri, K. E., Seitzinger, S., Reff, A., Lim, H. J., and Ervens, B.: Atmospheric oxalic acid and SOA production from glyoxal: results of aqueous photooxidation experiment, *Atmos. Environ.*, 41, 7588–7602, 2007.
- Carmichael, G. R., Sakurai, T., Streets, D., Hozumi, Y., Ueda, H., Park, S. U., Fung, C., Han, Z., Kajino, M., Engardt, M., Bannet, C., Hayami, H., Sartelet, K., Holloway, T., Wang, Z., Kannari, A., Fu, J., Matsuda, K., Thongboonchoo, N., and Amann, M.: MICS-Asia II: the model intercomparison study for Asia phase II methodology and overview of findings, *Atmos. Environ.*, 42, 3468–3490, 2008.
- Chen, F. and Dudhia, J.: Coupling an advanced land-surface/ hydrology model with the Penn State/ NCAR MM5 modeling system. Part I: Model description and implementation, *Mon. Weather Rev.*, 129, 569–585, 2001.
- Clarke, A. D., Shinozuka, Y., Kapustin, V. N., Howell, S., Huebert, B., Doherty, S., Anderson, T., Covert, D., Anderson, J., Hua, X., Moore II, K. G., McNaughton, C., Carmichael, G. R., and Weber, R.: Size distributions and mixtures of dust and black carbon aerosol in Asian outflow: physicochemistry and optical properties, *J. Geophys. Res.*, 109, D15S09, doi:10.1029/2003JD004378, 2004.

Development of RAQM2 and Asian aerosol mixing type simulation

M. Kajino et al.

Title Page

Abstract

Introduction

Conclusions

References

Tables

Figures

⏪

⏩

◀

▶

Back

Close

Full Screen / Esc

Printer-friendly Version

Interactive Discussion



Development of RAQM2 and Asian aerosol mixing type simulation

M. Kajino et al.

Title Page

Abstract

Introduction

Conclusions

References

Tables

Figures

◀

▶

◀

▶

Back

Close

Full Screen / Esc

Printer-friendly Version

Interactive Discussion



Clarke, A. D., Owens, S. R., and Zhou, J.: An ultrafine sea-salt flux from breaking waves: implications for cloud condensation nuclei in the remote marine atmosphere, *J. Geophys. Res.*, 111, D06202, doi:10.1029/2005JD006565, 2006.

Deushi, M. and Shibata, K.: Development of an MRI chemistry-climate model ver.2 for the study of tropospheric and stratospheric chemistry, *Pap. Meteorol. Geophys.*, 62, 1–46, 2011.

DOE, 1994: Handbook of methods for the analysis of the various parameters of the carbon dioxide system in sea water. Version 2, edited by: Dickson, A. G. and Goyet, C., ORNL/CDIAC-74, 1994.

Dudhia, J.: Numerical study of convection observed during the winter monsoon experiment using a mesoscale two-dimensional model, *J. Atmos. Sci.*, 46, 3077–3107, 1989.

Edney, E. O., Kleindienst, T. E., Lewandowski, M., and Offenberg, J. H.: Updated SOA chemical mechanism for the Community Multiscale Air Quality model. EPA 600/X-07/025, US Environ. Prot. Agency, Durham, N. C., 2007.

Foley, K. M., Roselle, S. J., Appel, K. W., Bhawe, P. V., Pleim, J. E., Otte, T. L., Mathur, R., Sarwar, G., Young, J. O., Gilliam, R. C., Nolte, C. G., Kelly, J. T., Gilliland, A. B., and Bash, J. O.: Incremental testing of the Community Multiscale Air Quality (CMAQ) modeling system version 4.7, *Geosci. Model Dev.*, 3, 205–226, doi:10.5194/gmd-3-205-2010, 2010.

Fountoukis, C. and Nenes, A.: ISORROPIA II: a computationally efficient thermodynamic equilibrium model for K^+ - Ca^{2+} - Mg^{2+} - NH_4^+ - Na^+ - SO_4^{2-} - NO_3^- - Cl^- - H_2O aerosols, *Atmos. Chem. Phys.*, 7, 4639–4659, doi:10.5194/acp-7-4639-2007, 2007.

Fuchs, N. A.: *The Mechanics of Aerosols*, Pergamon Press, Oxford, 1964.

Giglio, L., Randerson, J. T., van der Werf, G. R., Kasibhatla, P. S., Collatz, G. J., Morton, D. C., and DeFries, R. S.: Assessing variability and long-term trends in burned area by merging multiple satellite fire products, *Biogeosciences*, 7, 1171–1186, doi:10.5194/bg-7-1171-2010, 2010.

Grell, G. A. and Devenyi, D.: A generalized approach to parameterizing convection combining ensemble and data assimilation techniques, *Geophys. Res. Lett.* 20, 1693, doi:10.1029/2002GL015311, 2002.

Guazzotti, S. A., Coffee, K. R., and Prather, K. A.: Continuous measurements of size-resolved particle chemistry during INDOEX-Intensive Field Phase 99, *J. Geophys. Res.*, 106, 28607–28628, 2001.

Guenther, A., Karl, T., Harley, P., Wiedinmyer, C., Palmer, P. I., and Geron, C.: Estimates of global terrestrial isoprene emissions using MEGAN (Model of Emissions of Gases and

**Development of
RAQM2 and Asian
aerosol mixing type
simulation**

M. Kajino et al.

Title Page

Abstract

Introduction

Conclusions

References

Tables

Figures

◀

▶

◀

▶

Back

Close

Full Screen / Esc

Printer-friendly Version

Interactive Discussion

Aerosols from Nature), *Atmos. Chem. Phys.*, 6, 3181–3210, doi:10.5194/acp-6-3181-2006, 2006.

Han, Z., Ueda, H., Matsuda, K., Zhang, R., Arao, K., Kanai, Y., and Hasome, H.: Model study on particle size segregation and deposition during Asian dust events in March 2002, *J. Geophys. Res.*, 109, D19205, doi:10.1029/2004JD004920, 2004.

Han, Z., Ueda, H., and Matsuda, K.: Model study of the impact of biogenic emission on regional ozone and effectiveness of emission reduction scenarios over Eastern China, *Tellus B*, 53, 171–191, 2005.

Han, Z., Ueda, H., and Sakurai, T.: Model study on acidifying wet deposition in East Asia during wintertime, *Atmos. Environ.*, 40, 2360–2373, 2006.

Han, Z.: A regional air quality model: evaluation and simulation of O₃ and relevant gaseous species in East Asia during spring 2001, *Environ. Modell. Softw.*, 22, 1328–1336, 2007.

Hirsikko, A., Nieminen, T., Gagné, S., Lehtipalo, K., Manninen, H. E., Ehn, M., Hörrak, U., Kerminen, V.-M., Laakso, L., McMurry, P. H., Mirme, A., Mirme, S., Petäjä, T., Tammet, H., Vakkari, V., Vana, M., and Kulmala, M.: Atmospheric ions and nucleation: a review of observations, *Atmos. Chem. Phys.*, 11, 767–798, doi:10.5194/acp-11-767-2011, 2011.

Hong, S.-Y. and Lin, J.-O. J.: The WRF single-moment 6-class microphysics scheme (WSM6), *J. Korean Meteorol. Soc.*, 42, 129–151, 2006.

Ishikawa, H.: Mass-consistent wind model as a meteorological preprocessor for tracer transport models, *J. Appl. Meteorol.*, 33, 733–743, 1994.

Jacobson, M. Z. and Ginnebaugh, D. L.: Global-through-urban nested three-dimensional simulation of air pollution with a 13 600-reaction photochemical mechanism, *J. Geophys. Res.*, 115, D14304, doi:10.1029/2009JD013289, 2010.

Janjic, Z. I.: Nonsingular implementation of the Mellor-Yamada level 2.5 scheme in the NCEP Medo model, *Off. Note*, 437, 61 pp., Natl. Cent. for Environ. Predict., Camp Springs, Md.

Kajino, M., Ueda, H., Satsumabayashi, H., and An, J.: Impacts of the eruption of Miyakejima Volcano on air quality over far east Asia, *J. Geophys. Res.*, 109, D21204, doi:10.1029/2004JD004762, 2004.

Kajino, M., Ueda, H., Satsumabayashi, H., and Han, Z.: Increase in nitrate and chloride deposition in east Asia due to increased sulfate associated with the eruption of Miyakejima Volcano, *J. Geophys. Res.*, 110, D18203, doi:10.1029/2005JD005879, 2005.

Kajino, M., Ueda, H., and Nakayama, S.: Secondary acidification: Changes in gas-aerosol partitioning of semivolatile nitric acid and enhancement of its deposition due

Development of RAQM2 and Asian aerosol mixing type simulation

M. Kajino et al.

Title Page

Abstract

Introduction

Conclusions

References

Tables

Figures

⏪

⏩

◀

▶

Back

Close

Full Screen / Esc

Printer-friendly Version

Interactive Discussion

to increased emission and concentration of SO_x , *J. Geophys. Res.*, 113, D03302, doi:10.1029/2007JD008635, 2008.

Kajino, M.: MADMS: Modal Aerosol Dynamics model for multiple Modes and fractal Shapes in the free-molecular and near-continuum regimes, *J. Aerosol Sci.*, 42, 224–248, 2011.

5 Kajino, M. and Kondo, Y.: EMTACS: Development and regional-scale simulation of a size, chemical, mixing type, and soot shape resolved atmospheric particle model, *J. Geophys. Res.*, 116, D02303, doi:10.1029/2010JD015030, 2011.

Kang, J.-Y., Yoon, S.-C., Shao, Y., and Kim, S.-W.: Comparison of vertical dust flux by implementing three dust emission schemes in WRF/Chem., *J. Geophys. Res.*, 116, D09202, doi:10.1029/2010JD014649, 2011.

10 Katata, G., Nagai, H., Wrzesinsky, T., Klemm, O., Eugster, W., and Burkard, R.: Development of a land surface model including cloud water deposition on vegetation, *J. Appl. Meteor. Climatol.*, 47, 2129–2146, 2008.

15 Katata, G., Nagai, H., Zhang, L., Held, A., Serça, D., and Klemm, O.: Development of an atmosphere-soil-vegetation model for investigation of radioactive materials transport in the terrestrial biosphere, *Prog. Nucl. Sci. Technol.*, 2, online available: <http://www.aesj.or.jp/publication/pnst002/data/530-537.pdf>, last access: 28 May 2012, 530–537, 2011.

Kirsch, A. A. and Fuchs, N. A.: Studies on fibrous aerosol filters. III. Diffusional deposition of aerosols in fibrous filters, *Ann. Occup. Hyg.*, 11, 299–304, 1968.

20 Kuang, C., McMurry, P. H., McCormick, A. V., and Eisele, F. L.: Dependence of nucleation rates on sulfuric acid vapor concentration in diverse atmospheric locations, *J. Geophys. Res.* 113, D10209, doi:10.1029/2007JD009253, 2008.

Kulmala, M. and Kerminen, V.-M.: On the formation and growth of atmospheric nanoparticles, *Atmos. Res.*, 90, 132–150, 2008.

25 Kurokawa, J., Ohara, T., Uno, I., Hayasaki, M., and Tanimoto, H.: Influence of meteorological variability on interannual variations of springtime boundary layer ozone over Japan during 1981–2005, *Atmos. Chem. Phys.*, 9, 6287–6304, doi:10.5194/acp-9-6287-2009, 2009.

Lin, Y.-L., Farley, R. D., and Orville, H. D.: Bulk parameterization of the snow field in a cloud model, *J. Clim. Appl. Meteorol.*, 22, 1065–1092, 1983.

30 Lohmann, U. and Diehl, K.: Sensitivity studies of the importance of dust ice nuclei for the indirect aerosol effect on stratiform mixed-phase clouds, *J. Atmos. Sci.*, 63, 968–982, 2010.

Development of RAQM2 and Asian aerosol mixing type simulation

M. Kajino et al.

Title Page

Abstract

Introduction

Conclusions

References

Tables

Figures

⏪

⏩

◀

▶

Back

Close

Full Screen / Esc

Printer-friendly Version

Interactive Discussion



Madronich, S.: Photodissociation in the atmosphere: 1. Actinic flux and the effects of ground reflections and clouds, *J. Geophys. Res.*, 92, 9740–9752, doi:10.1029/JD092iD08p09740, 1987.

Mlawer, E. J., Taubman, S. J., Brown, P. D., Iacono, M. J., and Clough, S. A.: Radiative transfer for inhomogeneous atmosphere, RRTM, a validated correlated-k model for the long wave, *J. Geophys. Res.*, 102, 16663–16682, doi:10.1029/97JD00237, 1997.

Myneni, R. B., Hoffman, S., Knyazikhin, Y., Privette, J. L., Glassy, J., Tian, Y., Wang, Y., Song, X., Zhang, Y., Smith, G. R., Lotsch, A., Friedl, M., Morisette, J. T., Votava, P., Nemani, R. R., and Running S. W.: Global products of vegetation leaf area and fraction absorbed PAR from year one of MODIS data, *Remote Sens. Environ.*, 83, 214–231, 2002.

Nagashima, T., Ohara, T., Sudo, K., and Akimoto, H.: The relative importance of various source regions on East Asian surface ozone, *Atmos. Chem. Phys.*, 10, 11305–11322, doi:10.5194/acp-10-11305-2010, 2010.

Ohara, T., Akimoto, H., Kurokawa, J., Horii, N., Yamaji, K., Yan, X., and Hayasaka, T.: An Asian emission inventory of anthropogenic emission sources for the period 1980–2020, *Atmos. Chem. Phys.*, 7, 4419–4444, doi:10.5194/acp-7-4419-2007, 2007.

Peters, K. and Eiden, R.: Modelling the dry deposition velocity of aerosol particles to a spruce forest, *Atmos. Environ. A*, 26, 2555–2564, 1992.

Petroff, A. and Zhang, L.: Development and validation of a size-resolved particle dry deposition scheme for application in aerosol transport models, *Geosci. Model Dev.*, 3, 753–769, doi:10.5194/gmd-3-753-2010, 2010.

Pleim, J. E. and Chang, J. S.: A non-local closure model for vertical mixing in the convective boundary layer, *Atmos. Environ. A*, 26, 965–981, 1992.

Pruppacher, H. R. and Klett, J. D.: *Microphysics of Clouds and Precipitation*, Kluwer Acad., Norwell, Mass., 1997.

Sekiyama, T. T., Tanaka, T. Y., Shimizu, A., and Miyoshi, T.: Data assimilation of CALIPSO aerosol observations, *Atmos. Chem. Phys.*, 10, 39–49, doi:10.5194/acp-10-39-2010, 2010.

Skamarock, W. C., Klemp, J. B., Dudhia, J., Gill, D. O., Barker, D. M., Duda, M. G., Huang, X. Y., Wang, W., and Powers, J. G.: A description of the advanced research WRF version 3, Tech. Note, NCAR/TN~ 475 + STR, Natl. Cent. for Atmos. Res., Boulder, Colo., 125 pp., 2008.

Song C. H. and Carmichael, G. R.: A 3-D modeling investigation of the evolution processes of dust and sea-salt particles in east Asia, *J. Geophys. Res.*, 106(D16), 18131–18154, 2001.

emissions in 2006 for the NASA INTEX-B mission, Atmos. Chem. Phys., 9, 5131–5153, doi:10.5194/acp-9-5131-2009, 2009.

Zhang, Y., McMurry, P. H., Yu, F., and Jacobson, M. Z.: A comparative study of nucleation parameterizations: 1. Examination and evaluation of the formulations, J. Geophys. Res., 115, D20212, doi:10.1029/2010JD014150, 2010.

Zhu, A., Ramanathan, V., Li, F., and Kim, D.: Dust plumes over the Pacific, Indian and Atlantic Oceans: Climatology and radiative impact, J. Geophys. Res., 112, doi:10.1029/2007JD008427, 2007.

ACPD

12, 13405–13456, 2012

Development of RAQM2 and Asian aerosol mixing type simulation

M. Kajino et al.

Title Page

Abstract

Introduction

Conclusions

References

Tables

Figures

⏪

⏩

◀

▶

Back

Close

Full Screen / Esc

Printer-friendly Version

Interactive Discussion



Development of RAQM2 and Asian aerosol mixing type simulation

M. Kajino et al.

Title Page

Abstract

Introduction

Conclusions

References

Tables

Figures

⏪

⏩

◀

▶

Back

Close

Full Screen / Esc

Printer-friendly Version

Interactive Discussion



Table 2. Aerosol categories and their tracers in the RAQM2 model.

Category number	Category name	Physical components						Chemical compositions					
1	ATK	M_0	M_2	–	–	–	–	–	SO_4^{2-}	NH_4^+	NO_3^-	Cl^-	H_2O
2	ACM	M_0	M_2	UID	–	OA	–	–	SO_4^{2-}	NH_4^+	NO_3^-	Cl^-	H_2O
3	AGR	M_0	M_2	UID	BC	OA	–	–	SO_4^{2-}	NH_4^+	NO_3^-	Cl^-	H_2O
4	COR	M_0 M_0^{AGR}	M_2	UID	BC	OA	DU	SS	SO_4^{2-}	NH_4^+	NO_3^-	Cl^-	H_2O

Development of RAQM2 and Asian aerosol mixing type simulation

M. Kajino et al.

Title Page

Abstract

Introduction

Conclusions

References

Tables

Figures

⏪

⏩

◀

▶

Back

Close

Full Screen / Esc

Printer-friendly Version

Interactive Discussion



Table 3. Rules for transfer of the three moments and chemical mass concentrations from one category to another due to intercategory coagulation and mode merging.

Rule Number	Rule
Intercategory coagulation	
1	1.ATK + 2.ACM → 2.ACM
2	1.ATK + 3.AGR → 3.AGR
3	1.ATK + 4.COR → 4.COR
4	2.ACM + 3.AGR → 3.AGR
5	2.ACM + 4.COR → 4.COR
6	3.AGR + 4.COR → 4.COR
Mode merging	
7	(swelling) 1.ATK → 2.ACM
8	(shrinking) 2.ACM → 1.ATK

Development of RAQM2 and Asian aerosol mixing type simulation

M. Kajino et al.

Table 4. Description of the EANET remote sites and the CHAAMS site used in this study. Each station is depicted in Fig. 1.

	Longitude (E)	Latitude (N)	Altitude (m a.s.l.)	Characteristics	X	Y	MT	AT	AT-PM _{2.5}	FP	AMS
1. Rishiri	141°12′	45°07′	40	Remote	68	48	1h	1h	1h	2w	N.A.
2. Tappi	140°21′	41°15′	105	Remote	69	41	1h	1h	N.A.	2w	N.A.
3. Ogasawara	142°13′	27°05′	230	Remote	77	16	1h	1h	N.A.	1w	N.A.
4. Sado	138°24′	38°14′	136	Remote	67	35	1h	1h	N.A.	2w	N.A.
5 Oki	133°11′	36°17′	90	Remote	60	30	1h	1h	1h	2w	N.A.
6. Hedo & CHAAMS	128°15′	26°52′	60	Remote	54	12	1h	1h	N.A.	2w	1h

X,Y: Model grid number; MT: meteorological parameters, AT: automatically monitored (NO_x, O₃, SO₂, PM₁₀; PM_{2.5} is only available at Rishiri and Oki), FP: filter pack method (Aerosol inorganic components), AMS: aerosol mass spectrometer, only available at CHAAMS. CHAAMS is located within the same premises as the EANET Hedo station. 1h: hourly, 1w: weekly, 2w: 2 weekly.

Title Page

Abstract

Introduction

Conclusions

References

Tables

Figures

⏪

⏩

◀

▶

Back

Close

Full Screen / Esc

Printer-friendly Version

Interactive Discussion

Development of RAQM2 and Asian aerosol mixing type simulation

M. Kajino et al.

Title Page

Abstract

Introduction

Conclusions

References

Tables

Figures

⏪

⏩

◀

▶

Back

Close

Full Screen / Esc

Printer-friendly Version

Interactive Discussion



Table 5. Statistical analysis for comparison between all EANET data of observation and simulation for 2006.

	Unit	Number of data	Median (Obs.)	Median (Sim.)	RMSE	<i>R</i>	FAC2 ^a	FAC5 ^b
Daily mean bulk gas concentrations (AT) ^d								
O ₃ ^c	ppbv	2093	50.3	51.2	16.9	0.47	0.96	1.00
SO ₂	ppbv	2052	0.17	0.25	0.70	0.52	0.36	0.64
NO _x	ppbv	1819	0.80	0.58	1.1	0.49	0.52	0.86
1- or 2-weekly bulk concentrations of chemical compounds (FP) ^e								
Nss-SO ₄ ²⁻	μg m ⁻³	152	1.9	1.3	1.9	0.70	0.46	0.80
T-NH ₄ ⁺	μg m ⁻³	138	0.71	0.45	0.69	0.52	0.50	0.81
T-NO ₃ ⁻	μg m ⁻³	144	0.92	1.8	2.2	0.59	0.47	0.87
T-Cl ⁻	μg m ⁻³	144	3.7	2.8	4.2	0.13	0.42	0.89
Na ⁺	μg m ⁻³	144	2.3	1.4	2.5	0.13	0.38	0.85
Nss-Ca ²⁺	μg m ⁻³	152	0.056	0.11	0.24	0.55	0.38	0.67
Daily mean PM _{2.5} and PM ₁₀ concentration and their ratios (AT)								
PM _{2.5}	μg m ⁻³	696	8.8	5.2	10.8	0.45	0.52	0.87
PM ₁₀	μg m ⁻³	2141	17.7	8.3	19.1	0.65	0.45	0.81
PM _{2.5} /PM ₁₀	–	674	0.57	0.49	0.26	0.018	0.83	1.00

^a Fraction of data that satisfy a factor of 2.

^b Fraction of data that satisfy a factor of 5.

^c Daily maximum 8 h mean.

^d Measured by automatic instruments.

^e Measured by the filter pack method.

Development of RAQM2 and Asian aerosol mixing type simulation

M. Kajino et al.

Title Page

Abstract

Introduction

Conclusions

References

Tables

Figures

⏪

⏩

◀

▶

Back

Close

Full Screen / Esc

Printer-friendly Version

Interactive Discussion



Table 6. Statistical analysis for comparison between observation and simulation at the Hedo EANET and CHAAMS stations.

	unit	Number of data	Median (Obs.)	Median (Sim.)	RMSE	<i>R</i>	FAC2	FAC5
Daily PM ₁ concentrations (AMS) ^a								
PM ₁ -nss-SO ₄ ²⁻	μg m ⁻³	199	4.2	1.3	4.4	0.57	0.28	0.72
PM ₁ -NH ₄ ⁺	μg m ⁻³	199	1.0	0.34	1.0	0.56	0.28	0.70
PM ₁ -NO ₃ ⁻	μg m ⁻³	199	0.088	0.080	0.15	0.30	0.53	0.90
PM ₁ -Cl ⁻	μg m ⁻³	197	0.027	0.016	0.088	0.097	0.26	0.58
2-weekly bulk concentrations of chemical compounds (FP) ^b								
Nss-SO ₄ ²⁻	μg m ⁻³	22	5.9	2.0	3.0	0.83	0.32	0.86
T-NH ₄ ⁺	μg m ⁻³	20	1.4	0.47	0.91	0.56	0.20	0.80
T-NO ₃ ⁻	μg m ⁻³	22	1.7	2.6	1.7	0.49	0.72	1
T-Cl ⁻	μg m ⁻³	22	8.2	2.8	5.6	0.35	0.22	0.86
Na ⁺	μg m ⁻³	22	5.1	1.6	3.6	0.30	0.22	0.86
Nss-Ca ²⁺	μg m ⁻³	22	0.14	0.11	0.19	0.74	0.55	0.81
2-weekly PM ₁ to total concentration ratios (AMS/FP)								
Nss-SO ₄ ²⁻	–	12	0.85	0.66	0.32	–	0.92	1
T-NH ₄ ⁺	–	12	0.81	0.71	0.26	–	0.92	1
T-NO ₃ ⁻	–	12	0.054	0.035	0.027	–	0.75	1
T-Cl ⁻	–	12	0.0038	0.0080	0.0082	–	0.33	0.67

^a Measured by quadrupole aerosol mass spectrometer (Aerodyne Research Inc., Q-AMS).

^b Measured by the filter pack method.

Development of RAQM2 and Asian aerosol mixing type simulation

M. Kajino et al.

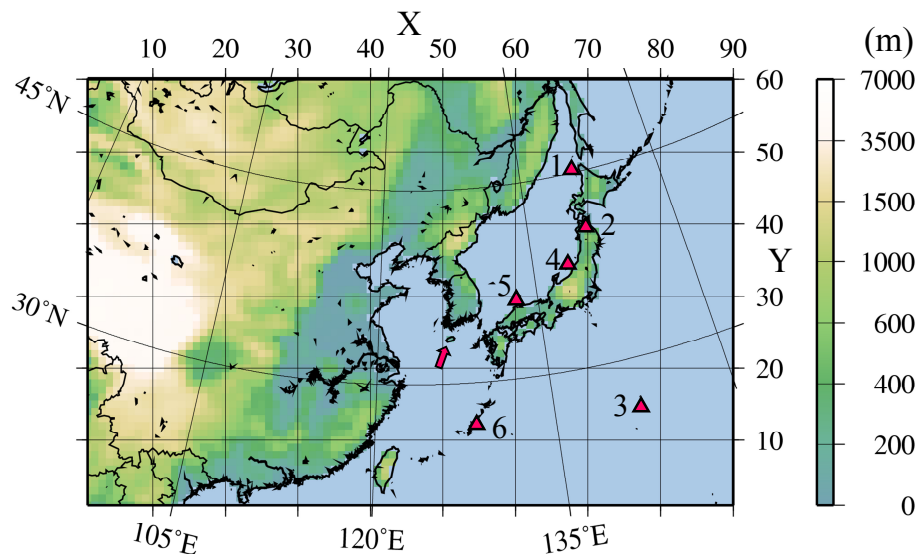


Fig. 1. Model domain showing terrestrial elevation (m) and the six Japanese EANET sites ((1) Rishiri, (2) Tappi, (3) Ogasawara, (4) Sado, (5) Oki, (6) Hedo) and the CHAAMS sites (located in the same premises as the EANET Hedo stations). The descriptions of the locations are given in Table 4. An arrow indicates the Gosan site on Jeju Island, Korea.

Title Page

Abstract

Introduction

Conclusions

References

Tables

Figures

◀

▶

◀

▶

Back

Close

Full Screen / Esc

Printer-friendly Version

Interactive Discussion

Development of RAQM2 and Asian aerosol mixing type simulation

M. Kajino et al.

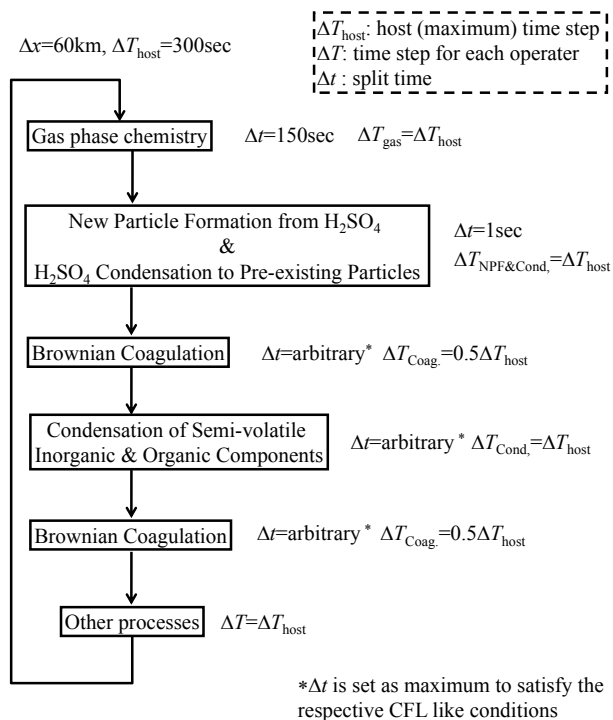


Fig. 2. Schematic illustration of operator splitting and time splitting for the RAQM2 aerosol dynamics module.

Title Page

Abstract

Introduction

Conclusions

References

Tables

Figures

◀

▶

◀

▶

Back

Close

Full Screen / Esc

Printer-friendly Version

Interactive Discussion

Development of RAQM2 and Asian aerosol mixing type simulation

M. Kajino et al.

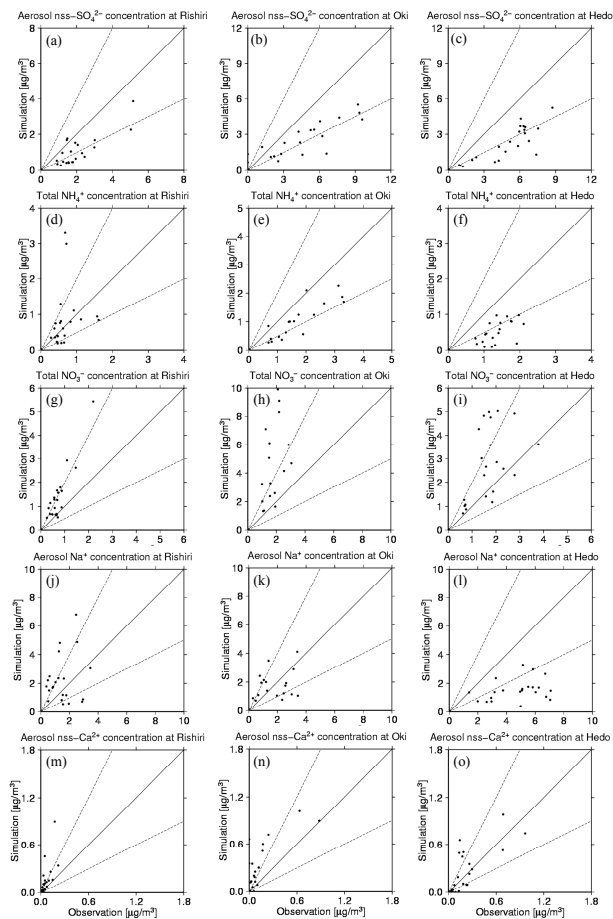


Fig. 3. Scatter diagram between observed and modeled concentrations of biweekly **(a–c)** nss-SO_4^{2-} , **(d–f)** T-NH_4^+ , **(g–i)** T-NO_3^- , **(j–l)** Na^+ , and **(m–o)** nss-Ca^{2+} at (left) Rishiri, (center) Oki and (right) Hedo. Solid lines denote the 1 : 1 line, and dashed lines denote the factor of 2 envelope.

[Title Page](#)
[Abstract](#)
[Introduction](#)
[Conclusions](#)
[References](#)
[Tables](#)
[Figures](#)
[Back](#)
[Close](#)
[Full Screen / Esc](#)
[Printer-friendly Version](#)
[Interactive Discussion](#)

Development of RAQM2 and Asian aerosol mixing type simulation

M. Kajino et al.

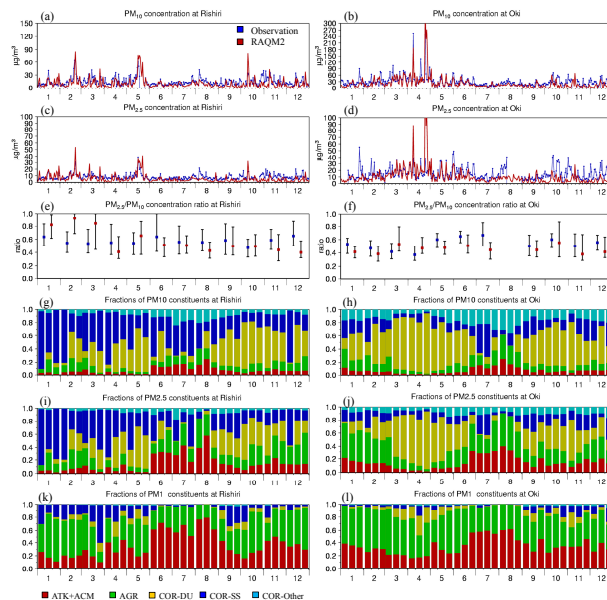


Fig. 4. Daily mean observed (blue) and modeled (red) concentrations of (a,b) PM₁₀, (c,d) PM_{2.5}, (e,f) PM_{2.5}/PM₁₀ concentration ratios (the median with 75 and 25 percentile values) and modeled constituent fractions of (g,h) PM₁₀, (i,j) PM_{2.5}, and (k,l) PM₁ concentrations at (left) Rishiri and (right) Oki. Among the constituents, ATK + ACM (red) is the total dry mass (SO₄²⁻, NH₄⁺, NO₃⁻, Cl⁻, UID and OA) of the ATK and ACM categories, AGR (green) is the total dry mass (UID, BC, OA, SO₄²⁻, NH₄⁺, NO₃⁻, and Cl⁻) of the AGR category, COR-DU (yellow) is the dust mass (DU) of the COR category, COR-SS (blue) is the sea-salt mass (SS + Cl⁻) in the COR category and COR-Other (sky blue) is the other components (UID, BC, OA, SO₄²⁻, NH₄⁺, and NO₃⁻) in the COR category.

Title Page

Abstract

Introduction

Conclusions

References

Tables

Figures

◀

▶

◀

▶

Back

Close

Full Screen / Esc

Printer-friendly Version

Interactive Discussion

Development of RAQM2 and Asian aerosol mixing type simulation

M. Kajino et al.

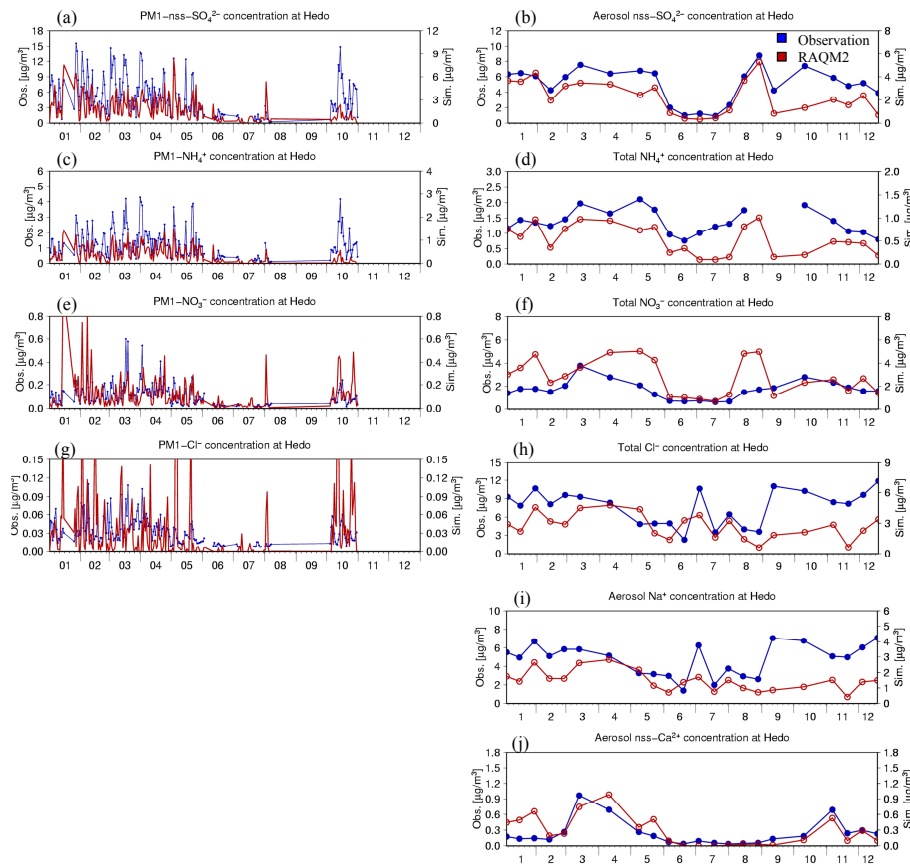


Fig. 5. (Left) daily mean AMS measured (blue, left axis) and modeled (red, right axis) PM₁ (a) nss-SO₄²⁻, (c) NH₄⁺, (e) NO₃⁻, and (g) Cl⁻ concentrations at Hedo (CHAAMS). (Right) biweekly FP measured and modeled (b) nss-SO₄²⁻, (d) T-NH₄⁺, (f) T-NO₃⁻, (h) T-Cl⁻, (i) Na⁺, and (j) nss-Ca²⁺ concentrations at Hedo (EANET).

Title Page	
Abstract	Introduction
Conclusions	References
Tables	Figures
◀	▶
◀	▶
Back	Close
Full Screen / Esc	
Printer-friendly Version	
Interactive Discussion	

Development of RAQM2 and Asian aerosol mixing type simulation

M. Kajino et al.

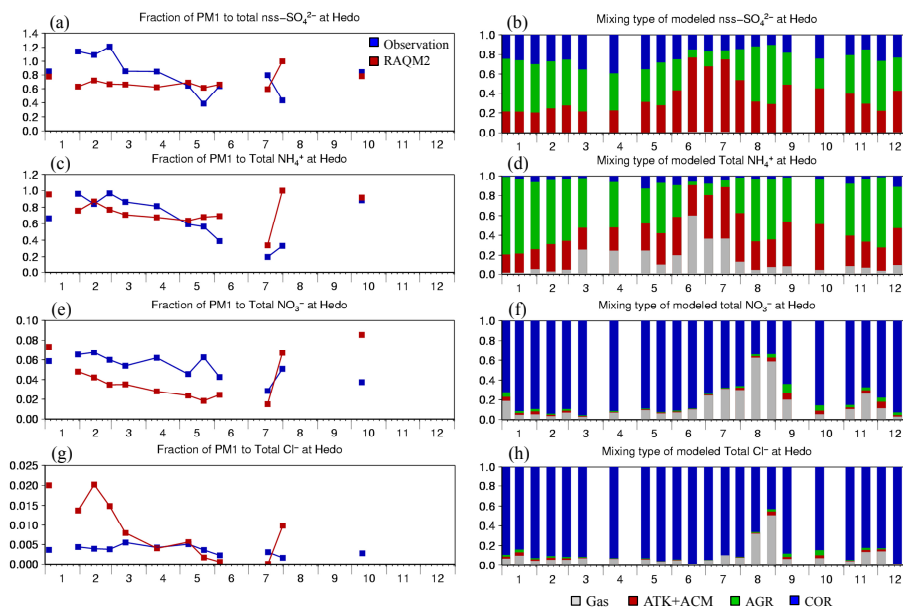


Fig. 6. (Left) biweekly mean PM_{10} to total (gas plus aerosol) concentration ratios and (Right) the modeled fractions of gas phase (grey), ATK + ACM category (red), AGR category (green), and COR category (blue) aerosols of **(a,b)** nss-SO_4^{2-} , **(c,d)** T-NH_4^+ , **(e,f)** T-NO_3^- , and **(g,h)** T-Cl^- at Hedo.

[Title Page](#)
[Abstract](#)
[Introduction](#)
[Conclusions](#)
[References](#)
[Tables](#)
[Figures](#)
[⏪](#)
[⏩](#)
[⏴](#)
[⏵](#)
[Back](#)
[Close](#)
[Full Screen / Esc](#)
[Printer-friendly Version](#)
[Interactive Discussion](#)